UNIVERSIDADE FEDERAL DO CEARÁ
CENTRO DE CIÊNCIAS
DEPARTAMENTO DE QUÍMICA ORGÂNICA E INORGÂNICA
PROGRAMA DE PÓS-GRADUAÇÃO EM QUÍMICA

EVERTON LUCAS DE LIMA RAMOS

INJECTABLE HYDROGEL BASED ON OXIDIZED GALACTOMANNAN FROM *Delonix regia* AND N-SUCCINYL CHITOSAN REINFORCED BY CHITIN NANOCRYSTALS

FORTALEZA
2021

EVERTON LUCAS DE LIMA RAMOS

INJECTABLE HYDROGEL BASED ON OXIDIZED GALACTOMANNAN FROM *Delonix regia* AND N-SUCCINYL CHITOSAN REINFORCED BY CHITIN NANOCRYSTALS

Tese apresentada ao Programa de Pós-graduação em Química da Universidade Federal do Ceará como requisito parcial à obtenção do título de Doutor em Química.
Área de concentração: Química

Orientadora: Profª. Judith Pessoa de Andrade Feitosa

FORTALEZA

2021

Dados Internacionais de Catalogação na Publicação
Universidade Federal do Ceará
Sistema de Bibliotecas
Gerada automaticamente pelo módulo Catalog, mediante os dados fornecidos pelo(a) autor(a)

R142i Ramos, Everton Lucas de Lima.
Injectable hydrogel based on oxidized galactomannan from delonix regia and n-succinyl chitosan reinforced by chitin nanocrystals / Everton Lucas de Lima Ramos. – 2021.
86 f. : il. color.

Tese (doutorado) – Universidade Federal do Ceará, Centro de Ciências, Programa de Pós-Graduação em Química, Fortaleza, 2021.
Orientação: Profa. Dra. Judith Pessoa de Andrade Feitosa.

1. Hidrogel injetável. 2. Galactomanana. 3. Quitosana. 4. Quitina. 5. Agente de reforço. I. Título.
CDD 540

EVERTON LUCAS DE LIMA DE RAMOS

INJECTABLE HYDROGEL BASED ON OXIDIZED GALACTOMANNAN FROM *Delonix regia* AND N-SUCCINYL CHITOSAN REINFORCED BY CHITIN NANOCRYSTALS

Tese apresentada ao Programa de Pós-Graduação em Química da Universidade Federal do Ceará como requisito parcial à obtenção do título de Doutor em Química.
Área de concentração: Química

Aprovada em: __/__/____.

BANCA EXAMINADORA

_____
Prof.ª Dra. Judith Pessoa de Andrade *Feitosa (Orientadora)*
Universidade Federal do Ceará (UFC)

_____
Prof.ª Dra. Jeanny da Silva Maciel
Universidade Federal do Ceará (UFC)

_____
Prof. Dr. Adriano Lincoln Albuquerque Mattos
Embrapa Agroindústria Tropical

_____
Prof.ª Dra. Durcilene Alves da Silva
Universidade Federal do Piauí (UFPI)

_____
Prof.ª Dra. Fábia Karine Andrade
Universidade Federal do Ceará (UFC)

Aos meus pais que tanto me apoiaram ao longo desta jornada.

ACKNOWLEDGEMENTS

My concept of faith changed a lot during this journey, but today I am sure that if I did what I did and got to where I arrived, it was thanks to all the blessings that were given to me by God. This was not an easy journey. More than scientific knowledge, this period within such a renowned institution, among such remarkable people, taught me a plenty of things that could not be found in books. A remarkable moment, an odd moment.

Thank you, Professor Judith, for all that you have me taught, for your endless patience and for believing that I could it. Without your guidance, I would not be here today.

My parents are a fundamental part of my education, they were the ones who first believed in me and invested in my education. My thanks to them and I hope that one day I will be able to repay everything that was given to me.

My three dear sisters who have always been with me and who although I am not so close, I know that they still cheer for me.

I need to give a special thanks to my wonderful wife. She has been with me all this time since graduation until today and always motivated me to keep trying and trying. It was a difficult period, a lot has changed in the meantime, but with her by my side I was able to feel more comfortable and safer. If I am here today, it is thanks to your intellectual help and mostly emotional support. Thank you so much for everything my love.

More than chemical knowledge, this little moment here among so special people taught me that we can learn things out the syllabus. The conversations and those great moment cannot and will not be forgotten. We need strong bonds, those that really stay with us and will do real difference in our life. So, I would like to say thank you so much for those that were side me, help me a lot always I need. For all my good friends from LabPol (Laboratório de Polímeros): Natália, Fabrício, Venicios, Rodrigo, Maria, Aline, Williane, Ana Rosa, Fernanda, Irisvan, Rhamon, Ribamar, Felipe, Leonira, Matheus, Neto, Raelle, Rayanne, Túlio, Brener, Nadia, Joan, Adison, I leave my thanks and I hope that one day we can be together again and remember all these moments. As Christopher McCandless once said : “Happiness only real when shared”, and I could not choose better partners to share my happiness. I'm sorry if I forgot someone.

Ludmilla was of fundamental importance for carrying out many of the experiments described throughout this work. Without your help I could not develop this work. My thanks also to Benício, who although not here but in Brazil, helped me a lot in the beginning of this journey.

I would like to thank Coordenação de Aperfeiçoamento de Pessoal de Nível Superior (CAPES), for granting the scholarship.

To the Graduate Program in Chemistry at UFC for the opportunities offered, for the physical support, the faculty.

I would like to thank CENAUREMN for the analysis of nuclear magnetic resonance.

I would like to thank the central analyst for the scanning electron microscopy analysis.

I would like to grateful all the people that directly or indirectly contribute for the elaboration of this work.

“All these moments will be lost in time, like tears in rain.
Time to die.”
(Rutger Hauer, From Blade Runner, 1982)

RESUMO

Entre os *scaffolds* comumente utilizados na abordagem da engenharia de tecidos, os hidrogéis vêm ganhando bastante destaque nas últimas décadas. Os hidrogéis injetáveis, ou formados *in situ*, são definidos como biomateriais em que os precursores são injetados na forma líquida e, em seguida, solidificam, ou seja, geleificam no local da administração. A utilização de hidrogéis para aplicações biomédicas baseados em materiais de partida como polissacarídeos é bastante atraente, tendo em vista que tais materiais tem boa compatibilidade com sistemas biológicos. Entretanto, hidrogéis de polissacarídeos tem problemas relacionados as baixas propriedades mecânicas. Uma alternativa para contornar esta problemática seria a adição de agentes de reforço ao longo da matriz do hidrogel. Portanto, neste trabalho, apresentamos a síntese e caracterização de hidrogéis injetáveis baseados em galactomanana de *Delonix regia* oxidada e N-succinil quitosana (ambas 3% m/v) reforçados pela adição de pequenas quantidades de nanocristais de quitina. As modificações dos polissacarídeos foram confirmadas por análise espectroscopica na região do infravermelho. Macroscopicamente, o hidrogel sem os nanocristais apresentou aspecto translúcido, enquanto os hidrogéis reforçados apresentaram aspecto levemente opaco, distribuição uniforme dos nanocristais sem qualquer ponto de agregação aparente. Pelas modificações realizadas, pode-se supor que o mecanismo de reticulação dos hidrogéis envolveu a formação de ligações cruzadas do tipo base de Schiff (C=N) entre os grupos aldeído da galactomanana oxidada e os grupos amino remanescente da N-succinil quitosana. Os nanocristais ficaram fisicamente presos e dispersos por toda a matriz, provavelmente pelo estabelecimento de ligações de hidrogênio com os grupos hidroxila das cadeias adjacentes, agindo como um reforço para criar um material mais resiliente. A análise de microscopia eletrônica de varredura revelou que os hidrogéis tem uma estrutura de poros com diâmetros e formas variadas, o que favorece a troca gasosa e transporte de nutrientes. O intumescimento realizado em água foi cerca de 10-12 vezes maior do que quando em tampão fosfato (pH 7,4). Apesar das soluções contendo os nanocristais apresentarem viscosidade visivelmente mais elevada, a sua adição não comprometeu a injetabilidade dos hidrogéis como demonstrado pelo ensaio usando seringa 26G (0.45x13mm). O tempo de geleificação dos hidrogéis variou entre 377 e 1157 s, o que está de acordo com os critérios estabelecidos na literatura para hidrogéis injetáveis. A adição dos nanocristais melhorou um pouco as propriedades mecânicas dos hidrogéis com 0,2 e 0,4% de agente de carga. Para aqueles hidrogéis com maiores quantidades de nanocristais, o efeito observado foi o contrário. Os

ensaios biológicos *in vitro* utilizados para avaliar a citotoxicidade dos hidrogéis demonstrou que os sistemas analisados apresentaram viabilidade acima de 90% e com isso podem ser considerados seguros para um possível ensaio *in vivo.* Maiores ensaios tornam-se necessários para uma completa caracterização destes sistemas, mas diante dos resultados obtidos, pode-se inferir que os hidrogéis produzidos têm potencialidade para serem empregados como biomateriais, com diferentes aplicações, como o encapsulamento de células ou liberação controlada de fármacos.

Palavras-chave: hidrogel injetável; galactomanana; quitosana; quitina; agente de reforço.

ABSTRACT

Among the scaffolds commonly used to approach tissue engineering, hydrogels have been gaining prominence in recent decades. Injectable hydrogels, or formed in situ, are defined as biomaterials in which the precursors are injected in liquid form and then solidify, that is, they gel in the administration site. The use of hydrogels for biomedical applications based on starting materials such as polysaccharides is quite attractive, considering that such materials have good compatibility with biological systems. However, polysaccharide hydrogels have problems related to low mechanical properties. An alternative to overcome this problem would be the addition of reinforcing agents along the hydrogel matrix. Therefore, in this work, we present the synthesis and characterization of injectable hydrogels based on oxidized galactomannan from Delonix regia and N-succinyl chitosan (both 3% w / v) reinforced by the addition of small amounts of chitin nanocrystals. The polysaccharide changes were confirmed by spectroscopic analysis in the infrared region. Macroscopically, the hydrogel without the nanocrystals showed a translucent aspect, whereas the reinforced hydrogels showed a slightly opaque aspect, uniform distribution of the nanocrystals without any apparent aggregation point. From the modifications made, it can be assumed that the crosslinking mechanism that led to the formation of hydrogels involved the formation of cross-links of the Schiff base type (C = N) between the aldehyde groups of the oxidized galactomannan and the remaining amino groups of the N- succinyl chitosan. The nanocrystals were physically trapped and dispersed throughout the matrix, probably by establishing hydrogen bonds with the hydroxyl groups of the adjacent chains, acting as a reinforcement to create a more resilient material. The scanning electron microscopy analysis revealed that the hydrogels have a pore structure with different diameters and shapes, which favors the gas exchange and transport of nutrients. The swelling performed in water was about 10-12 times greater than when in phosphate buffer. Although the solutions containing the nanocrystals present visibly higher viscosity, their addition did not compromise the injectability of the hydrogels as shown by the test using a 26G syringe (0.45x13mm). The gelation time of the hydrogels varied between 377 and 1157 s, which is in accordance with the criteria established in the literature. The addition of nanocrystals did not significantly improve the mechanical properties for hydrogels with 0.2 and 0.4% filler and for those hydrogels with higher amounts of nanocrystals, the opposite effect was observed. The in vitro biological tests used to evaluate the cytotoxicity of the hydrogels showed that the analyzed systems showed viability above 90% and therefore can be considered safe for a possible in vivo test. Further tests are

necessary for a complete characterization of these systems, but given the results obtained, it can be inferred that the hydrogels produced have the potential to be used as biomaterials, with different applications, such as cell encapsulation or controlled drug release.

Keywords: injectable hydrogel; galactomannan; chitosan; chitin; reinforcing agent.

LIST OF FIGURES

SUMMARY

1 INTRODUCTION

1.1 Tissue engineering and Injectable hydrogels

Many health problems, including cardiovascular diseases, diabetes and osteoarthritis can't be treated effectively with the current clinical therapies due to a significant reduction in the level of tissue regeneration (GUAN et al., 2017). Every day thousands of people of all ages are hospitalized due to malfunctioning of some organ (HOSSEINKHANI; HONG; YU, 2013). The ever-increasing demand for organ donors to meet the needs of people on the waiting list will probably never be answered (ZHENG et al., 2018). According to the Brazilian Association of Organ Transplantation (BAOT), 10,377 transplants of solid organs, tissues and bone marrow were performed in the period between January and June 2021. In June of 2021 BAOT had 45,664 patients registered on the waiting list. The need for organs or tissues cannot be achieved through traditional methods of transplantation. Tissue engineering and regenerative medicine emerge as an alternative to change this situation (GUAN et al., 2017; MAO; MOONEY, 2015).

According to LANGER and VACANTI (1993), tissue engineering (TE) is an interdisciplinary field that applies the principles of engineering and life sciences to develop biological substituents that restore, maintain, or enhance the function of a tissue. TE is an emerging field that offers excellent opportunities for regenerative medicine.

The most common concept underlying TE is the combination of scaffolds or matrices, living cells and/or biologically active molecules for the production of supports that promote repair and regeneration of diseased tissues (ZHENG et al., 2018). This frequently used strategy involves the incorporation of appropriate cells (from a healthy tissue biopsy) into a support, which serves as a temporary extracellular matrix (ECM) until the cells produce a new matrix and the newly formed tissue can replace the support (MATHEW et al., 2018; GUAN et al, 2017) (**Figure 1**). Autologous cell therapy is performed using the patient's own cells, while allogeneic cell therapy uses donor cells (YANG et al., 2014).

Figure 1 - Diagram showing the most common strategy used in tissue engineering. In both approaches, the cells are initially collected from a biopsy, cultured *in vitro*, seeded into a well-designed scaffold, and transplanted into the patient either through injection, or via implantation at the desired site using surgery

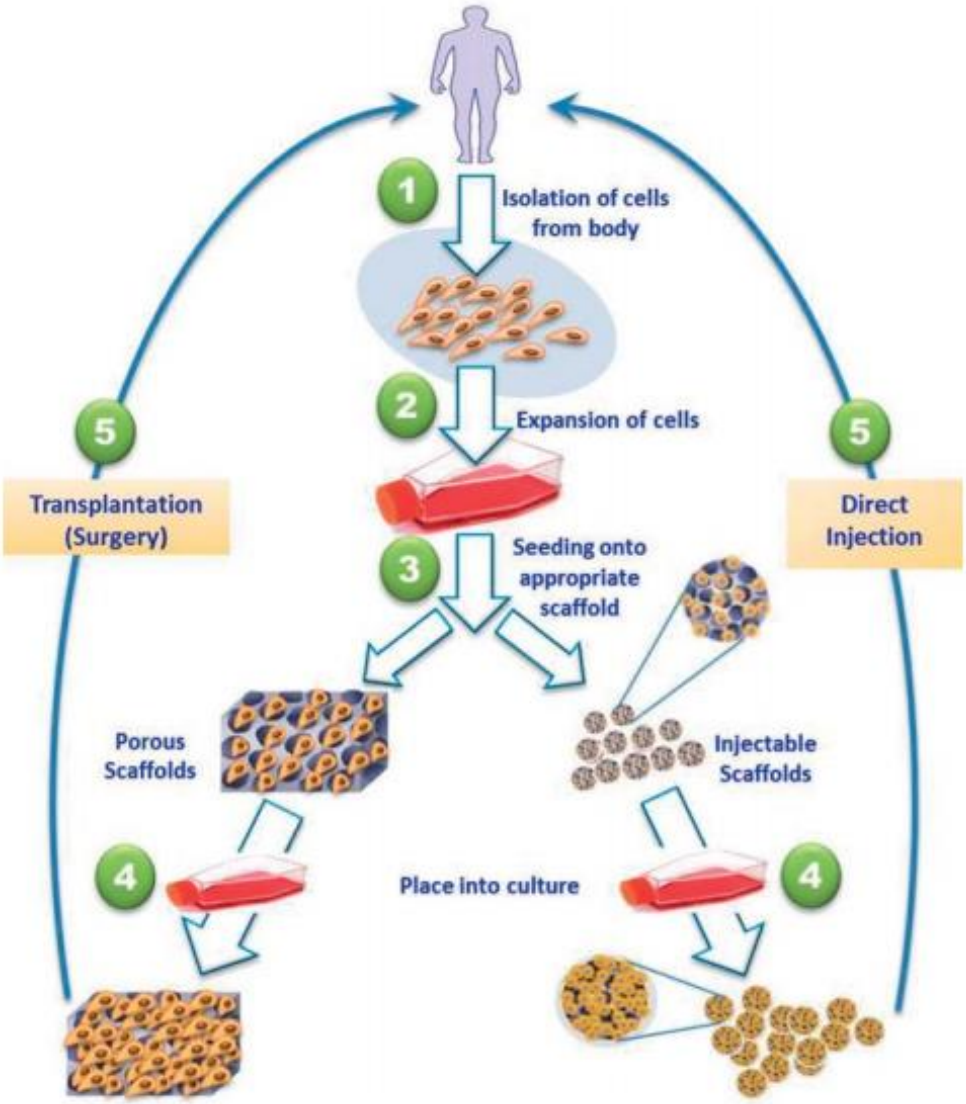

Source: El-Sherbiny and Yacoub, 2013.

The ECM is a composite of the secreted products of cells resident in all tissues and organs (SALDIN et al., 2017). The matrix molecules represent a diverse mixture of structural and functional proteins, glycoproteins and glycosaminoglycans among other molecules that are arranged in a structure that is unique to each anatomical location (LANGHANS, 2018; SALDIN et al., 2017). Due to the structural and functional complexity of ECM, the manufacture of an artificial and biomimetic organ *in vitro* remains a major challenge for tissue regeneration (AHADIAN et al., 2015; GUAN et al., 2017).

A widely used technique is the decellularization of natural ECM from allogeneic and xenogeneic sources (donor of different species, e.g. pigs), for the production of commercially available ECM (BROWN; BADYLAK, 2014). The process of decellularization consists of the removal of cells and debris from tissues and organs, while preserving the biochemical composition, biological activity, three-dimensional organization and integrity of the ECM (YOUNGSTROM et al., 2013). Nevertheless, the use of this procedure is not always successful, because the ECM from natural source has uncontrolled variability that can arise from the age, health and gender of individual sources (FITZPATRICK; MCDEVITT, 2015). For artificially produced scaffolds, the production of ECM constituents has been used as an indication that a support has conditions necessary for cell maintenance and proliferation (YAN et al., 2014).

A series of strategies are being applied to build biomaterials that can mimic the high degree of complexity of a native ECM like scaffolds, decellularization of tissues, bioprinted structures (LOEBEL et al., 2017; RANA et al., 2017). Between the broad spectrum of biomaterials with great potential to be applied as an artificial ECM, supports developed from hydrogels have received considerable attention due to their unique composition and structural similarities to natural ECM (Yue et al, 2015). Hydrogels are three-dimensional networks of hydrophilic polymers that can absorb water or biological fluids without dissolving because of their crosslinked structure (ZHANG; KHADEMHOSSEINI, 2017). There are many properties that make them attractive in the design of supports for biomedical application, including cytocompatibility, high water content, prolonged release of growth factors, and adjustable physical properties according to application (GUAN et al., 2017; HUNT et al., 2014).

Injectable hydrogels represent a subclass of hydrogels. The injectable hydrogels are based on the idea that certain biomaterial can be injected as liquid, and then form a solid gel *in situ* (ENCYCLOPEDIA OF NANOTECHNOLOGY, 2012) The hydrogel precursor solution can be introduced in a minimally invasive manner using a syringes or catheters, directly at the site of interest, reducing patient discomfort, infection risk, recovery time, and treatment cost (BAKAIC; SMEETS; HOARE, 2015).

In a general sense, these hydrogels are prepared by the combination of two polymeric solutions with reactive functional groups that interact between them to form a point of junction know as crosslinking. In some cases, a polymeric solution is mixed with the solution

of a low molecular mass molecule (e.g glutaraldehyde, adipic acid dihydrazide, formaldehyde etc) that joins two points of the polymer (PATENAUDE, SMEETS and HOARE, 2014).

A variety of crosslinking mechanism has been used to produce injectable hydrogel. Once injected, hydrogel formation occurs through physical crosslinking (electrostatic forces, hydrophobic interactions, hydrogen bonding, stereo-complex, π–π stacking, metal–ligand coordination) or by chemical crosslinking (photoirradiation, Schiff's base, Michael's addition, click reactions, oximes, enzyme-mediated reactions) (LIU et al., 2017) (**Figure 2**). Physical crosslinking offers the advantage of the absence of potential cytotoxicity chemical crosslinking agents besides provides reversible and weak linkages that can contribute to a self-healing property of the hydrogels. On the other hand, chemical crosslinking is formed by covalent bonds that are strongest, more stable and in general provides superior mechanical properties when compared with physical crosslinking (HU et al., 2019).

It is worth noting that not necessarily just one type of crosslinking can be used in the synthesis of an injectable hydrogel (YOUNG, RIAHINEZHAD and AMSDEN., 2019). There are a series of papers that described the combination of both chemical and physical methods to improve the mechanical characteristics of the hydrogel. For example, THAKUR et al, 2016, prepared an injectable shear-tinning hydrogel that was both chemically and physically crosslinked. They modified the structure of a kappa–carrageenan by introducing methacrylate groups that can be chemically crosslinked in the presence of UV irradiation. The physical entanglement between the chains was promoted by the addition of K^+, from KCl, that interact with the sulfate groups of kappa–carrageenan. Additionally, the authors also introduced nanoparticles of nanosilicates to reinforce the structure of the hydrogel.

PETER X. MA group has developed a series of injectable conductive hydrogels, based mainly on chemical cross-links between amines and aldehydes groups from natural occurring modified polymers. They proposed a system to drug release based on a hydrogel composed of oxidized dextran and chitosan-g-polyaniline. The obtained hydrogel had a short gelation time (45 to 444 s), was effective to load the drugs (amoxicillin and ibuprofen), present excellent antibacterial activity against *Escherichia coli* and *Staphylococcus aureus* and *in vivo* biocompatibility (QU et al., 2018). The same research group have been designed hydrogels for cardiac cell therapy (DONG et al 2016), wound dressing (QU et al, 2019) and mucoadhesive drug delivery systems (LIANG et al., 2019).

Figure 2 - Some of the common methods utilized to crosslinking injectable hydrogel. In the up side of figure are listed the chemical methods and in the down side are presented the physical

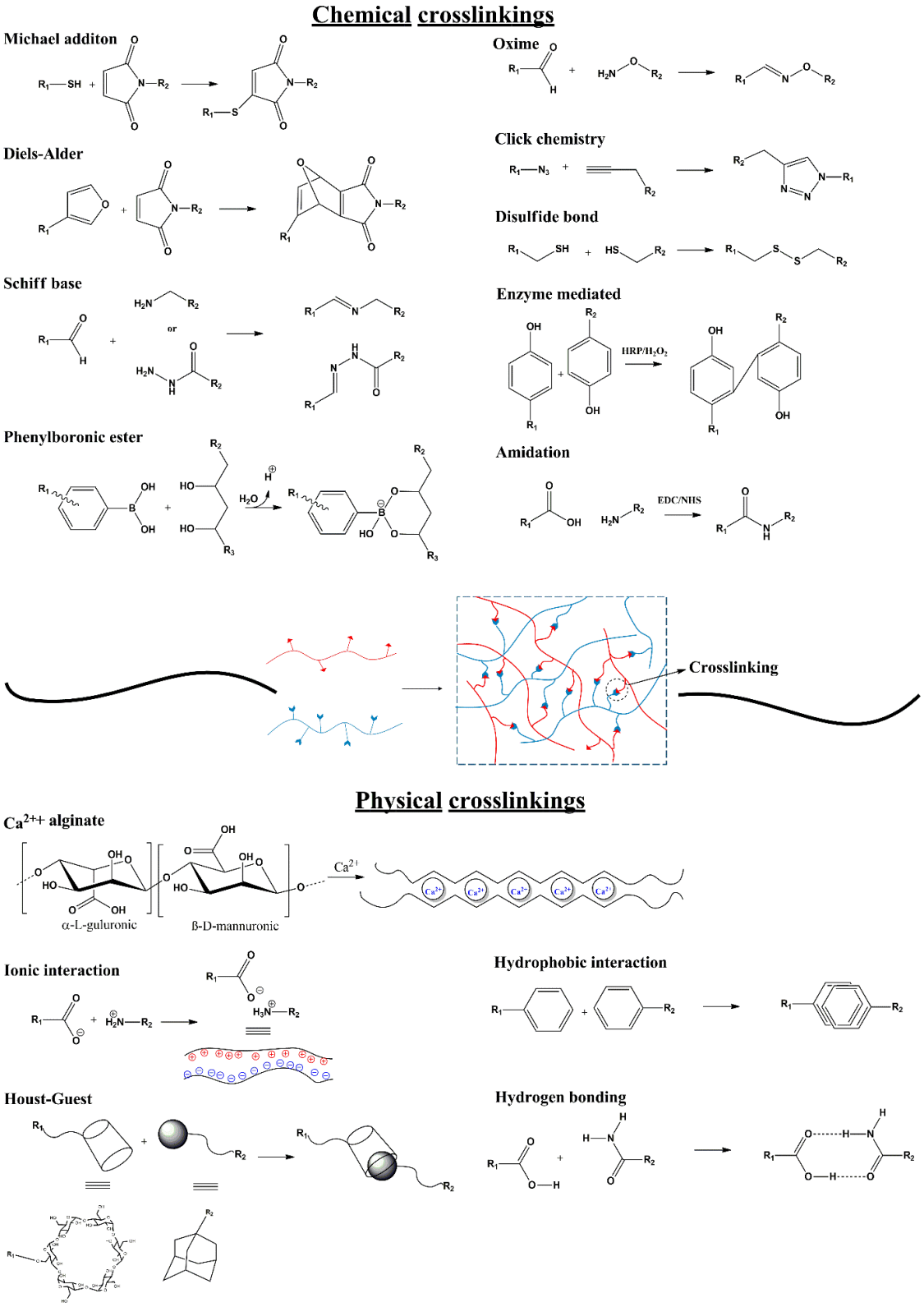

Another interesting crosslinking strategy is developed by BURDICK and coworkers. Their focus in the synthesis of shear-thinning hydrogels using host-guest complex

(physical crosslinking). Recently, the group have presented a protocol to build an injectable hydrogel from functionalized hyaluronic acid either with adamantanes (guest moieties) via controlled esterification or with β-cyclodextrins (host moieties) through amidation. This non-covalent approach between the derivatives allowed the hydrogel to experience breaking (shear-thinning behavior) when submitted to the high shear stress to pass through the syringe needle and then reassemble within few seconds (self-healing) upon cessation of shear (LOEBEL et al, 2017).

The search by injectable biomaterials (hydrogels, foams, cement etc) that can meet the needs of tissue engineering has increasing the interest of the academic community in recent years. A reflect this is the increasing number of papers published with this theme (**Figure 3**) by researchers of the areas of chemistry, biomaterials, biotechnology, regenerative medicine and others that focus on different aspects related to the synthesis, characterization, challenges and application in different fields, such as cartilaginous tissue engineering, drug delivery, stem cell therapies, bioink to 3D printing, bone regeneration (YOUNG, RIAHINEZHAD and AMSDEN, 2019; MATHEW et al, 2018; SINGH et al, 2018; LOEBEL et al, 2017; REAKASAME and BOCCACCINI, 2018). The number of publications with the term "injectable hydrogels" in 2018 was almost twice as high as in 2012 (456 versus 253). Until 2007, there has been a slight growth in the number of publications and, from 2008 and 2014, there has been a steeper increase.

Figure 3 - Number of publications per year (a) with the keywords "injectable hydrogel" or "injectable scaffold" between 1990-2019. The research was done in the Scopus database on May 20, 2019 and includes articles, reviews, books, book chapters, meetings, conference paper and letters

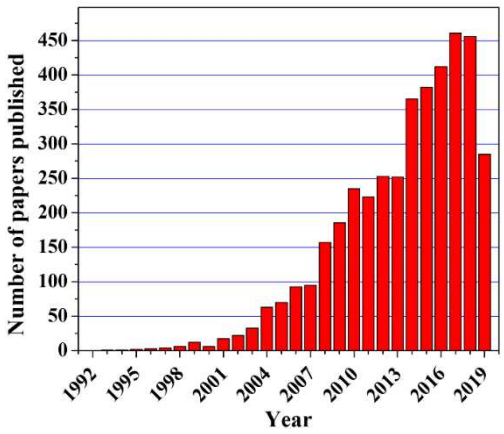

Injectable hydrogels have a series of advantages over preformed supports. In the case of preformed supports (scafffolds), prior knowledge of the shape and size of the defect or

cavity to be filled is necessary, and defects with irregular shapes and sizes can be problematic. In addition, invasive surgery is required to implantation of the support. The use of injectable hydrogels can overcome these limitations. The injectable nature of these systems makes it possible to add pharmaceutical agents and/or cells within them, resulting in a matrix that can fill any cavity, regardless of shape or size, with minimally invasive procedure and can (LI; RODRIGUES; TOMÁS, 2012; MATHEW et al., 2018).

Natural polymers, synthetic polymers and decellularized ECM or the combinations thereof, can be used for the preparation of injectable hydrogels. Synthetic polymer has advantages related with the batch-to-batch homogeneity and facility to control some properties (molar mass, polydispersion index). However, the absence of specific site to cells adheres and its non-biodegradable nature limits their utilization (YOUNG, RIAHINEZHAD and AMSDEN, 2019). Natural polymers (polysaccharides: chitosan, hyaluronic acid, cellulose, galactomannan, or proteins: gelatin, collagen, silk fibroin) have the advantage of biocompatibility and enzymatic biodegradability. They provide surface for cell adhesion, besides the fact that they can mimic many characteristics of the natural ECM and therefore has the potential to direct cell migration, growth and organization during tissue regeneration (MATHEW et al., 2018). An additional advantage associated with natural polymers is associated with their abundance and the variety of functional groups (OH, COOH, NH_2, SO_3H) that allows a myriad of chemical modifications.

Despite presenting a number of advantages, conventional hydrogels of natural polymers usually have poor mechanical properties and accelerated degradation, which limits their application in TE (XU; BRATLIE, 2018). By the addition of reinforcing agents, the properties of the hydrogel can be tailored to a variety of applications (YANG et al., 2013).

1.2 Chitin Nanocrystals as reinforcing agents

One of the main drawbacks associated with application of injectable hydrogels based in polysaccharides is related to their structural brittleness (YOUNG, RIAHINEZHAD and AMSDEN, 2019). The absence of appropriates mechanical properties can compromise a long-term application or that where a high mechanical resistance is required (e.g., cartilaginous tissue engineering, bone replacement) (LIU et al., 2016; SARKER et al., 2016).

A strategy commonly utilized to improve the mechanical properties of the hydrogels is the mix of one of the precursor solutions with a component, in nanometer scale

and sometimes in micrometric scale, that can reinforce the hydrogel matrix creating a composite material. This component can be covalently bound to the matrix hydrogel or added as a dopant that interacts physically with the hydrogel (PIANTANIDA et al, 2019). The one who interacts physically is the most common. The component is known as reinforcing agent, load bearing agent, or just filler, and can be of organic or inorganic nature.

As an example of organic microfiller, CHEN et al., 2017, prepared gelatin microspheres crosslinked with glutaraldehyde, in diameter varying to 73-88 μm, to reinforce (and delivery tetracycline hydrochloride) a hydrogel composed of oxidized alginate and carboxymethyl chitosan. They observed an increase of 66,5% on compressive modulus when compared with the hydrogel without microspheres beyond a better stability on the degradation assay.

SAKER et al, 2016, designed a composite scaffold by combination of oxidized alginate and type A gelatin (300 Bloom, porcine skin) chemically crosslinked. To the proposed scaffold, small quantities of bioactive glass (that act an inorganic filler) was added to enhance the mechanical properties. The pristine scaffold presented a compressive modulus of 135 kpa whereas the composites had their values increased to 304 and 417 kpa, for 1% and 5% of bioactive glass, respectively. Additional examples of inorganics filler normally used to reinforce matrix include hydroxyapatite, metal nanoparticles, halloysite nanotubes, carbon nanotubes and graphene oxide (DOMINGUES, GOMES and REIS, 2014).

Despite the widespread use of inorganic filler, there are some limitations related with their application that are the non-biodegradability, possible toxicity associated and processability. As an alternative to common inorganic filler, the utilization of natural derived fillers has gained attention.

Chitin nanocrystals and principally cellulose nanocrystals are polysaccharides widely applied as nanofillers (LIU et al.b, 2018; SILVA et al., 2018; WANG; CHEN; CHEN, 2017). Generally, the potential of a material to reinforce a matrix is directly related with their aspect ratio (ZENG et al, 2012). The higher the aspect ratio, the greater the potential of the material to reinforce the matrix. Therefore, because the physical appearance of chitin and cellulose nanocrystals under the transition electron microscopy (with large length and thin width), it is supposed that can act as a filler to polymeric matrices creating more resilient structures.

In fact, chitin nanocrystals have a longitudinal modulus of 41-60 GPa, while cellulose nanocrystals present a tensile strength is in the range of 7.5−7.7 GPa (DOMINGUES, GOMES and REIS, 2014; DUAN et al, 2018). Beyond the great potential to enhance the mechanical properties, polysaccharide nanocrystals also have excellent characteristics to application in biomedical field, such as biocompatibility and biodegradability, renewable nature, low cost and high aspect ratio (SCAFFARO et al., 2017; SHEN et al., 2016).

The application of cellulose nanocrystals as load bearing agents is well documented in literature, being the subject of some reviews (DOMINGUES, GOMES and REIS, 2014; DE FRANCE, CRANSTON and HOARE, 2020), while chitin nanocrystals have a few numbers of paper (in relative terms to cellulose nanocrystals) dedicated to it. Although it is the second most abundant biopolymer after cellulose, 6 to 8 million tons of chitin per year are produced worldwide (YAN; CHEN, 2015), there are few studies that explore the utilization of chitin nanocrystals as a reinforcing agent for preformed or injectable hydrogels.

As an example, HUANG et al., 2015, prepared a nanocomposite hydrogel from alginate and chitin whiskers. Hydrogels were formed by electrostatic interaction between chitin whiskers and alginate. The authors verified an enhance in compressive modulus of the composite hydrogels from 5.08 MPa to 13.72 MPa by the addition of chitin whiskers. Moreover, the presence of chitin whiskers contributed to increase the cytocompatibility of the composite hydrogel; unfortunately, these hydrogels were no in situ gellable.

Chitin is a polysaccharide that is mostly obtained mainly from the exoskeleton of crustaceans, but can be also extracted from mushroom, mollusk shells, and cell walls of fungi and yeast (ZHANG, ROLANDI 2017). Therefore, its production adds economic value to the exploitation of resources that once had no specific purpose and were discarded.

Structurally, chitin bears resemblance to cellulose, having as a differential the substituting group in C2 that can be an amine or a N-acetyl group. From a chemical viewpoint, chitin is defined as a co-polymer randomly formed by units of N-acetyl-glucosamine and N-glucosamine (deacetylated) held together through glyosidic bonds β-(1→4) (ZHANG, ROLANDI 2017) (**Figure 4**).

Figure 4 - Structural similarity between chitin and cellulose

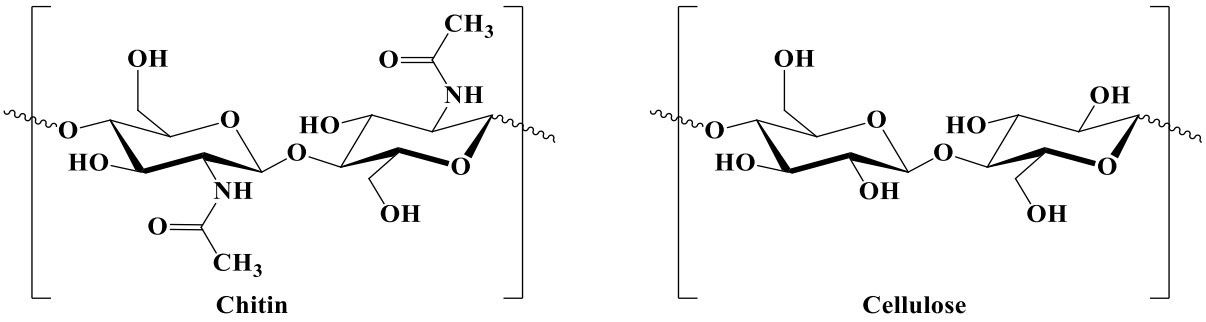

Chitin polymorphisms render three different arrangements of chain known as α, β and γ that differ from each other by the orientation and packaging of chitin molecules over each other. From these, α form is most common and is characterized by antiparallel chains that led to formation of strong hydrogen bonds between adjacent chain (RINAUDO 2006, DUAN et al, 2018).

Generally, the process to obtain the chitin, with at least one dimension on the nanometer scale, is made by using high-pressure homogenization (microfluidization), strong inorganic acids or by selective oxidation of primary alcohol groups in the presence of 2,2,6,6-tetramethylpiperidine-1-oxyl (TEMPO) radical followed by mechanical disintegration (YANG et al., 2020). Between these, the more common and widely used is that apply solutions of strong inorganic acid, like HCl or H_2SO_4, which removes the amorphous domain (deacetylated units). The crystalline domain is isolated at nanoscale and is generally known as nanocrystal, nanowhiskers or just as whisker (ZENG et al., 2012).

Here, it is important differentiate between nanofibers and nanocrystals. While to produce nanofibers are generally applied physical methods to disintegrate fibers, like ultrasonication, microfluidization or high-speed blending, nanocrystals pass through a chemical harsh process that consumes regions of high disorder (amorphous domain) and highly organized regions (crystalline domain) are isolated in nanometric scale. This differentiation is valid for both cellulose and chitin.

The CNC were first prepared by MARCHESSAULT in 1959 using HCl 2.5 N under reflux by 1h. In the year of 2001, PAILLET and DUFRESNE proposed for the first time the incorporation of chitin nanocrystals as reinforcing agent in a thermoplastic nanocomposite composed of latex. However, there is still a gap regarding the application of these fillers in composites for biomedical application.

Although chitin is the primary product of crustacean exoskeleton processing, this polysaccharide has industrial application in disagreement with its potential. On the other hand, chitin derivatives have been proposed to a series of applications. Chitosan represents the main product derivative from chitin and have great potential to be applied in different areas like biomedical field, wound dressings, antibacterial lining for bandages etc. (BELLICH et al., 2016).

1.3 Chitosan and N-succinyl chitosan

The production chain of chitin and chitosan represents a business model environmentally friendly since that they are obtained products of renewable nature and sustainable and contribute to the creation of a circular economy where the waste (mainly shrimp and crab shell) are converted in materials with much more associated value (BELLICH et al., 2016). In fact, almost 75% of total weight of these wastes ends up as by-products.

Chemically, Chitosan is a polysaccharide composed by units of N-acetyl-2-amino-2-deoxy-D-glucopyranose and 2-amino-2-deoxy-D-glucopyranose units linked by β-(1 → 4) glycosidic linkages and available in different grades of acetylation (MOREIRA et al., 2016; ZENG et al., 2012). It is a polymer having one amino group and two hydroxyl groups for each deacetylated glycosidic unit and in the case of acetylated unit there are two hydroxyl groups and one N-acetyl group.

Chitosan is obtained from chitin either by alkaline heat treatment or by enzymatic treatment, where some of the N-acetyl units are deacetylated, forming units with an amino (NH_2) group in their position (**Figure 5**). The main commercial source of chitin is shrimp, lobster and crab waste (HAMED; ÖZOGUL; REGENSTEIN, 2016). The chitin has limited applications due to its low solubility in aqueous solutions and the great most of the organic solvents. In contrast, chitosan is more versatile because of its solubility in acidic media (pH <6.0), biocompatibility, biodegradability, and low toxicity. The acids used for their dissolution include inorganic acids such as HCl and organic acids such as acetic acid and lactic acid. Chitosan is insoluble at neutral and alkaline pH. The mechanism of solubilization of chitosan involves the protonation of amino groups in glucosamine units leading to the formation of NH_3^+(BASHIR et al., 2015).

Figure 5 - Reaction involved in the process of obtaining chitosan from chitin

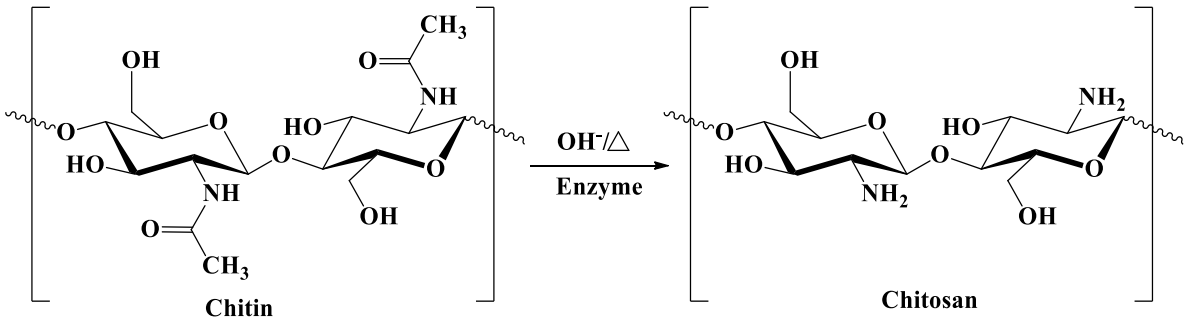

Chitosan jointly with its derivatives can be used to manufacture the most diverse types of biomaterials such as films, scaffolds, hydrogels, sponges, microspheres, nanoparticles, filaments, among others. However, in the case of biomedical applications, it is necessary that chitosan be soluble at physiological pH (7,4). This can be achieved by modifying its structure by insertion or formation of hydrophilic groups over the backbone. JAYAKUMAR et al., (2010), elaborated a review citing some available methodologies to produce soluble derivatives in aqueous solution of chitin and chitosan. The modifications mentioned in this work use the nucleophilic character of the amine nitrogen and the hydroxyl oxygen to attack reagents that have electrophilic regions, such as glyoxylic acid, monochloroacetic acid, levulinic acid, among others.

Among the modifications cited, one that draws attention is the production of N-succinyl chitosan because the obtained derivative has been reported as versatile biomaterial for biomedical applications (BASHIR et at, 2015). The reaction takes place between the amine groups of chitosan and the succinic anhydride. This modification amplifies the pH range at which chitosan can be solubilized and increases its biocompatibility of the derivative (BASHIR et al., 2015). The derivative O-succinyl chitosan can also be selectively produced, but for this a step of protecting the amino group is required (ZHANG et al., 2003).

The N-succinyl chitosan derivative has been utilized to produced hydrogel for prevent peritoneal adhesions (MITSUHASHI et al., 2019), soft tissue engineering (XING et al., 2019), removal of zinc and cationic dye from binary hazardous mixtures (KYZAS et al., 2015).

The water-soluble derivatives of chitosan can be used to produce injectable hydrogels by the crosslinking reaction with aldehyde groups of oxidized polysaccharides. This approach has been applied in a great number of publications, where most of the papers uses the derivative of chitosan produced by reaction with chloroacetic acid. Here, we chose N-succinyl

chitosan as a derivative due to the properties previously mentioned and because the number of works of this derivative in the literature is much smaller when compared to other hydrosoluble derivatives of chitosan such as carboxymethyl chitosan and carboxyethyl chitosan

1.4 Galactomannan and oxidation of polysaccharides

Like chitosan, galactomannan is also a natural polymer. Chemically, galactomannans are non-ionic hydrophilic heteropolysaccharides composed of linear chains of β-D-mannopyranose linked residues (1 → 4) partially substituted with linked α-D-galactopyranose side groups (1 → 6). (BARAK; MUDGIL, 2014; SINHA; KUMRIA, 2001) (**Figure 6**). They are mostly obtained from the endosperm of dicotyledonous seeds of numerous plants, particularly those of *Leguminosae* family.

Figure 6 - Representation of galactomannan structure showing its binding pattern between mannose and galactose units

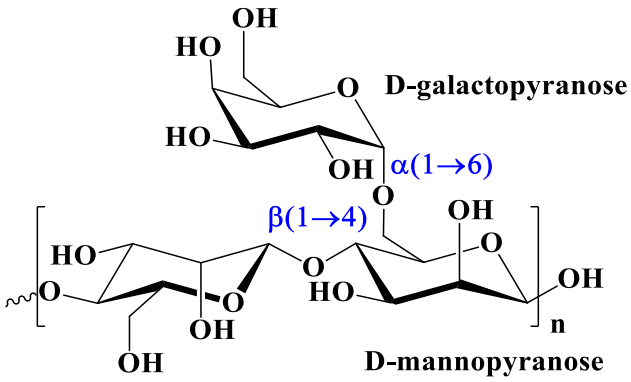

Approximately 90-100 tons of galactomannan are consumed per year around the world (PRAJAPATI et al., 2013). The absence of toxicity favors its use in the pharmaceutical, biomedical, cosmetic and food industries (Yadav and Maiti, 2020). There are several studies that show its versatility in the field of biomaterials. *Delonix regia* galactomannan, for example, has been proposed in literature for the preparation of scaffold for cells (SIQUEIRA et al., 2015), antimicrobial dressing (CHEIRMADURAI; THANIKAIVELAN; MURALI, 2016) and controlled release of bioactive substances (BETANCUR-ANCONA et al., 2011).

Despite the overall trend to use biopolymers to produce biological devices as hydrogels, nanoparticles etc, there is still a gap of research where galactomannans are the main product of such devices. Galactomannan is a widely available polymers that can be get by a price fraction when compared to other polymers like hyaluronic acid. Obviously that such polymer has some key characteristic that make it a specie of holy grail when we think about

biopolymers, but galactomannan has a series of OH groups that can be functionalized to mimetite the features of other polymers.

The OH groups to galactomannan can be modified to broaden the applications and properties of the derivative. For example, this group can be replaced by nonpolar portion to produce a more hydrophobic material or also it may be possible to attach more polar groups like carboxymethyl. Some commonly used derivatizations cited in literature are: sulfation (MOURA NETO et al., 2014), grafting with acrylic monomers (ABREU et al., 2016), acetylation (DIAS et al., 2016), oxidation with periodate ion, and some others. Among the modifications mentioned, periodic ion oxidation is notable for occurring in the absence of catalysts and in which the reaction product can be isolated by a simple dialysis step (MAIA et al., 2011).

Originally, periodate oxidation was used with the goal to analyze the chemical composition of complex carbohydrates. In addition to its primary utilization, periodate oxidation has now been extensively used to introduce aldehyde groups into the polysaccharide structure. The derivative can act as a crosslinking agent for natural (e.g., gelatin, collagen, chitosan, silk fibroin) or synthetic N-nucleophiles (hydrazide-functionalized poly(N-isopropylacrylamide-co-acrylic acid), carboxymethyl cellulose-*g*-adipic acid dihydrazide), through the formation of an imine (-CH=N-) linkage also known as Schiff's base (REAKASAME and BOCCACCINI., 2018).

Derivatives formed by the oxidation reaction have two aldehyde groups per glycosidic unit (the position of these groups varies according to the unit binding pattern) and is commonly known as dialdehyde. Dialdehyde polysaccharides are structures which act similarly to glutaraldehyde, reacting with amines to form imine bonds, but with the advantage of being less cytotoxic and to some extent more efficient (WANG et al., 2015; XU et al., 2013).

The pattern of insertion of the aldehyde groups along the chain of a polysaccharide is intrinsically related to how the glycosidic units bind to each other (**Figure 7**). Oxidation with the periodate ion is selective for vicinal diols (side by side hydroxyls); will consume one mole of periodate. Structures exhibiting isolated hydroxyls cannot react with IO_4^- (**Figure 7b**). In the case of glycosidic units containing three adjacent hydroxyls (**Figure 7d** and **7e**), a double oxidation will occur followed by the release of 1 mole of formic acid. This reaction consumes two moles of periodate. **Figure 7** shows the selectivity of the periodate ion *versus* glycosidic units with different binding patterns.

The dialdehydes have been produced from a variety of polysaccharides, such as hyaluronic acid (DOMINGUES et al., 2015), cellulose (SIRVIÖ et al., 2014), alginate (REAKASAME; BOCCACCINI, 2018), galactomannan (RINAUDO, 2010). Among the aforementioned polysaccharides, galactomannan dialdehydes are still not widely used, with only a few papers reporting their synthesis and use as a crosslinking agent (RINAUDO, 2010).

Figure 7 - Selectivity of sodium periodate reaction with substituted sugar units in different positions. a) linked residues (1 → 2), b) (1 → 3), c) (1 → 4), d) (1 → 6) and e) non-reducing end

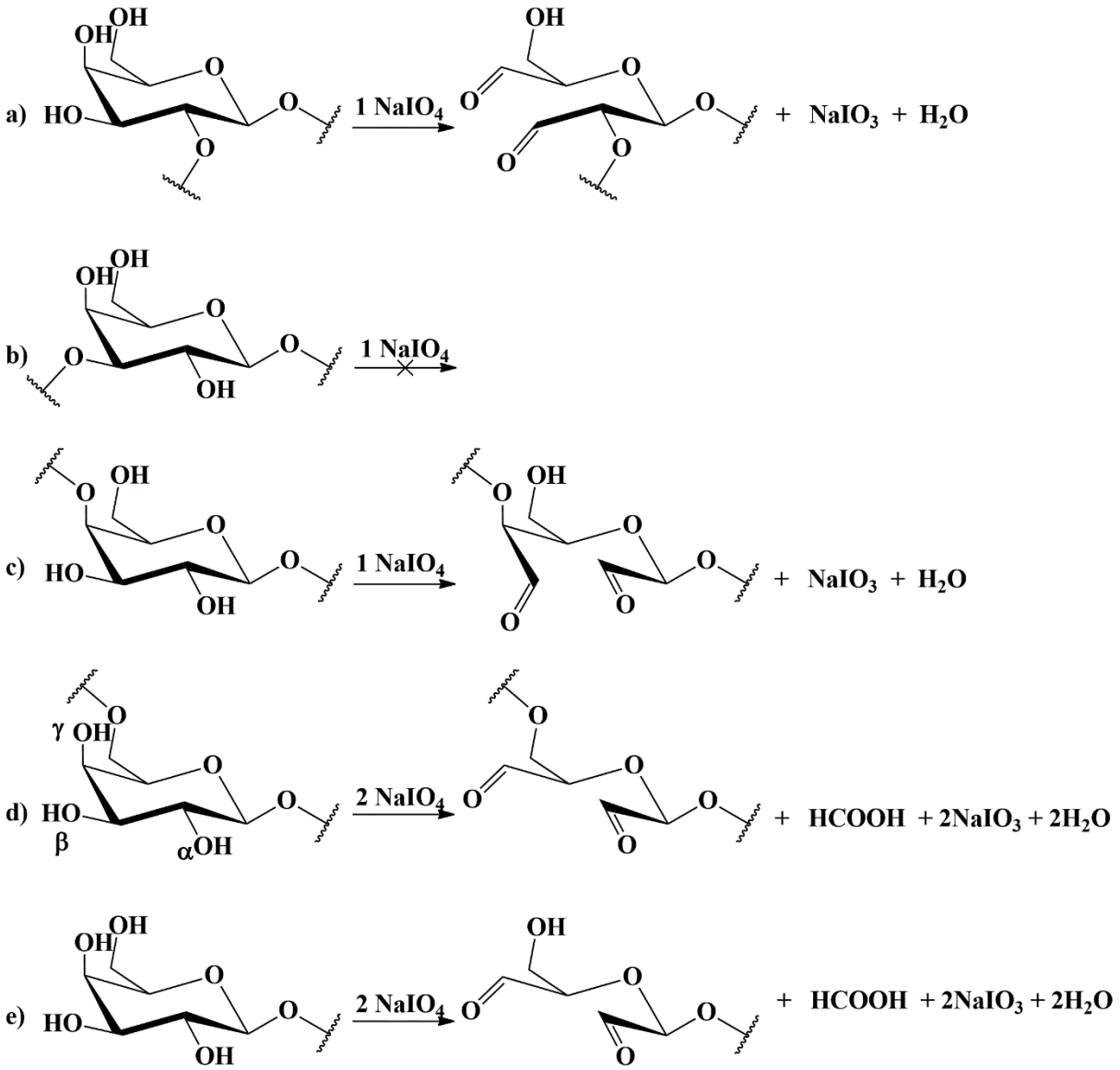

2 OBJECTIVES

2.1 General objective

- Prepare injectable hydrogels by the reaction of oxidized galactomannan and succinylated chitosan reinforced with of chitin nanocrystals.

2.2 Specific objectives

- Oxidize the galactomannan of *Delonix regia* using sodium periodate;
- Prepare the soluble derivative of chitosan by reaction with succinic anhydride;
- Prepare chitin nanocrystals via acid hydrolysis with HCl;
- Characterize the derivatives obtained by FTIR, NMR;
- Formulate hydrogels by the combination of oxidized galactomannan, modified chitosan and chitin nanocrystals;
- Evaluate the effect of chitin nanocrystals on the mechanical and physicochemical properties of the hydrogels;
- Evaluate the cytocompatibility of the hydrogels obtained.

3 MATERIALS AND METHODS

3.1 Materials

Ethanol (Synth), acetone (Synth), sodium periodate (Vetec), ethylene glycol, hydroxylamine hydrochloride (Vetec), sodium hydroxide (Vetec), acetic acid (Synth), methanol (Synth), succinic anhydride (Sigma), potassium hydroxide (Synth), hydrogen peroxide (Vetec), hydrochloric acid (Synth). Galactomannan was obtained from seeds of *Delonix regia*; chitin and chitosan were obtained from Polymar.

3.2 Extraction of galactomannan

The seeds of *Delonix regia* (100 g) were selected, washed, and placed in a Petri dish coated with cotton wool moistened with distilled water and overlaid with another layer of moistened cotton. The plate was autoclaved for 60 min under pressure (1.0 to 1.5 bar) for seed swelling. The seeds were separated manually in endosperm, tegument, and cotyledon. Endosperms were placed to hydrate overnight under stirring (1:15 w/v relative to seed mass). The endosperms were crushed, centrifuged at 6.000 rpm (3.663 g) for 30 min at 25 ° C and the supernatant collected and precipitated in two volumes of ethanol. The residue underwent a new extraction like the previous one to improve yield. The precipitate was filtered through a sintered plate funnel (N° 4) under vacuum and washed three times with alcohol and acetone. The galactomannan obtained was macerated, dried in a mortar with hot air, heavy and stored at room temperature. The sample was coded as unmodified galactomannan (UnGM).

3.3 Oxidation of galactomannan

The UnGM was oxidized by the method described by Yan et al., 2014. The conversion of the OH to CHO groups in the monosaccharide units of galactomannan was carried out using sodium periodate as an oxidizing agent. 1.0 g (0.0062 mol of monosaccharide units) of galactomannan was dissolved in 200 mL of distilled water and stirred for 24 h. To this solution a quantity of sodium periodate ($NaIO_4$) sufficient to obtain the degree of oxidation of 50% was added. The reactional system was covered with an aluminum foil to prevent photoinduced decomposition of the periodate ion and the reaction was run for 6 h. The reaction was stopped by adding ethylene glycol in a molar ratio of 1:1 to $NaIO_4$. The solution was dialyzed against distilled water for 4 days on cellulose membrane with exclusion limit of $12.4x10^3$ g/mol, and then the oxidized derivative was dried by lyophilization. The absence of periodate in the dialysate was accompanied by the conductance of the water. The sample was

encoded as oxidized galactomannan (OxGM). The pH variation of the solution was monitored during the first 2 h of reaction to verify the release of formic acid.

To obtain only the soluble fraction, an additional procedure was performed. The OxGM was dissolved in PBS buffer (pH 7.4, 10 mmol) at 3% w/v concentration and the solution was heated (60 min, 50 ° C). The resulting solution was centrifuged (6000 rpm; 10 min) to remove the insoluble fraction. The supernatant was frozen in liquid nitrogen and lyophilized. This was the material used for the preparation of the hydrogels.

3.4 Determination of oxidation degree of oxidized galactomannan

The degree of oxidation, i.e., the percentage of oxidized monosaccharide units, was determined by measuring the aldehyde content using the method proposed by Zhao and Heindel, 1991. A mass of 0.100 g of lyophilized OxGM was dissolved in 25 mL of a solution 0.25 mol/L hydroxylamine hydrochloride ($NH_2OH \cdot HCl$). The mixture was stirred at room temperature for 24 h. Conversion of aldehydes to oximes (C = N-OH) (**Figure 8**) was followed by titration of the liberated HCl with 0.1123 mol/L NaOH solution previously standardized with potassium biftalate. The change in pH with the volume of NaOH added was recorded. The number of moles of NaOH consumed is equivalent to the number of moles of aldehydes present in the sample. The volume of NaOH at the equivalence point was found by the second derivative of the titration curve. All determinations were done in triplicate.

The chemical equations 1-3 represent the reactions involved in the oxidation, titration and neutralization process. (1) oxidation of GM with $NaIO_4$, (2) reaction of OxGM with $NH_2OH \cdot HCl$, (3) neutralization of released HCl.

$$GM_{(aq)} + NaIO_{4(aq)} \rightarrow GM\text{-}(CHO)_{n\,(aq)} \quad (1)$$

$$GM\text{-}(CHO)_{n\,(aq)} + nH_2N\text{-}OH \cdot HCl_{(aq)} \rightarrow GM\text{-}(CH{=}N\text{-}OH)_{n\,(aq)} + nH_2O + nHCl_{\,(aq)} \quad (2)$$

$$HCl_{(aq)} + NaOH_{(aq)} \rightarrow NaCl_{(aq)} + H_2O_{(l)} \quad (3)$$

Figure 8 - Reaction between oxidized galactomannan and hydroxylamine hydrochloride

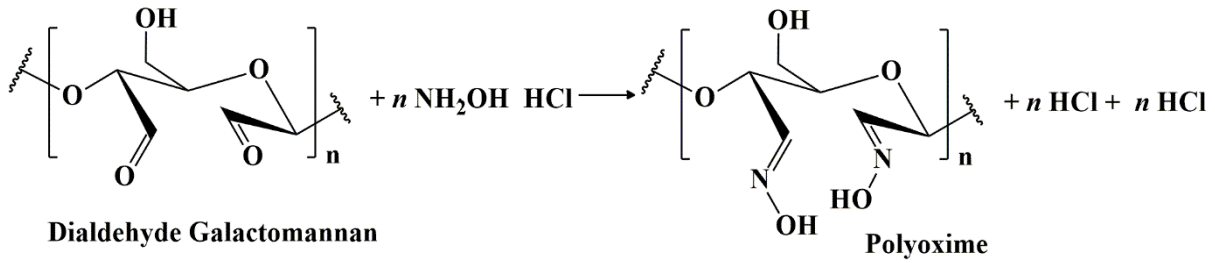

The equation (4) was used to calculate the degree of oxidation (Yan et al., 2014):

$$Oxidation\ degree = (162 \cdot V \cdot c \cdot 10^{-3})/2m \text{ x } 100\ \% \quad (4)$$

where V is the volume of NaOH solution consumed, in mL; c is the concentration of the NaOH solution in mol/L; m is the mass of GM-CHO, in grams; and 162 is the molar mass of the monosaccharide repeat unit (mannose and galactose) in g/mol.

3.5 Purification of chitosan

Chitosan was purified according to methodology described by Benamer, 2012, with some modifications. The chitosan was initially selected in a 100 mesh screen. 5.0 g of chitosan were dissolved in 500 mL of 2% (v/v) acetic acid and left under stirring for 24 h for complete dissolution. The solution was then centrifuged (15 min, 4500 rpm), filtered through sintered plate funnel N° 3 and then boiled for 15 min to denature and precipitate the proteins. The mixture was again centrifuged (15 min, 4500 rpm). The supernatant was removed and filtered through sintered plate funnel N° 3. The pH of the solution was adjusted to 10 with 1 mol/L NaOH to precipitate the chitosan from the aqueous phase. The chitosan precipitate was recovered by centrifugation and washed with deionized water to remove excess NaOH until the pH and conductivity values reached the pure water values. Chitosan was dried by lyophilization. The product was coded as chitosan.

3.6 Synthesis of N-succinyl chitosan

N-succinyl chitosan was synthesized according to methodology reported by Bashir et al, 2017, with some modifications. The purified chitosan (1.0 g) was placed in a 100 mL round bottom flask, dispersed with 500 mL of acetic acid solution (5.0% v/v) and kept under magnetic stirring at 60 °C for 45 min in a glycerin bath. Then, methanol (50 mL, 1.23 mol) was added to the mixture. Subsequently, the succinic anhydride (3.5 g, 0.025 mol) was dissolved in

30 mL of acetone and mixed with chitosan solution. The reaction was run for 48 h at 50 °C. After 48 h, the pH of the mixture was adjusted to 12 with a 1.0 mol/L NaOH solution and a clear solution was formed. Thereafter, the mixture was kept at room temperature for 24 hours. The final product was precipitated by the addition of ethanol (95%). The precipitate was isolated by centrifugation (5 min, 6000 rpm) and then washed several times with ethanol and acetone on a sintered plate funnel (N° 4) to remove these excesses of reagents. The derivative was dried at 70 °C in an oven for 3 h, stored at room temperature and coded as N-succinyl chitosan (NSC).

3.7 Characterization of oxidized galactomannan and N-succinyl chitosan

OxGM and NSC were characterized by Nuclear Magnetic Resonance (NMR) and Fourier Transform Infrared Spectroscopy (FTIR). NMR analyses were performed on a Bruker Avance DRX500 spectrometer (70°C, resonance frequencies 500 MHz to 1H). Samples (UnGM, OxGM and NSC) were dissolved in 600 µL of D_2O, followed by stirring for 24 h. Unmodified chitosan was dissolved in a mixture of 550 µL of D_2O and 50 µL of DCl. The solutions were transferred to 5 mm resonance tube. Sodium 2,2-dimethyl-2-silapentane-5-sulfonate (DSS) was used as the internal standard for chemical displacement. The spectra were treated with the BRUKER topspin software version 1.3. The FTIR spectra of the samples were determined using a Fourier Transform infrared spectrometer (IR trace-100) between 4000 and 400 cm^{-1}. Samples were prepared in KBr pellets. OxGM also had the molar mass distribution determined by gel permeation chromatography on Shimadzu LC-20AD equipment coupled to a refractive index detector (RID-10A). To perform the analysis a linear Polysep column (300x7.8 mm) was used with 0.1 mol/L $NaNO_{3(aq)}$ as the eluent. The measurements are made at 30 °C and flow rate is 1 mL/min. The injected volume of the samples was 50 µL.

3.8 Purification of chitin and preparation of chitin nanocrystals

The procedure for chitin purification and nanocrystals extraction was performed according to the methodology described by Paillet and Dufresne, 2001 with minor modifications. Before starting the purification process, the chitin flakes were crushed into a blender and then selected with a 35 mesh sieve. The obtained powder (10.0 g) was placed in a round bottom flask, KOH (5.0% w/v, 300 mL) was added, and the mixture was heated under stirring (100°C, 6 h) in a sand bath. The suspension was then kept at room temperature overnight under stirring, subsequently filtered through a sintered plate funnel (N° 3) and washed with distilled water. The chitin was then bleached with H_2O_2 (300 mL, 1.5% v/v) for 6 h at 80 °C.

The bleach solution was changed every two hours, followed by washing of the sample with distilled water. After bleaching, the suspension was maintained in a solution of KOH (5.0% w/v, 300 mL) for 48 h at room temperature to remove the residual proteins. The resulting suspension was washed with distilled water to remove excess KOH.

The purified chitin powder (10.0 g) was subjected to hydrolysis with HCl (3.0 mol/L, 6 h, 105 °C) under stirring in a round bottom flask. The ratio of HCl solution to chitin was 30 mL/g. After acid hydrolysis, the reaction was quenched by the addition of 1.0 L of deionized water and the suspension was allowed to decant overnight. The clear supernatant was discarded, and the remaining chitin suspension centrifuged (10 min, 6000 rpm) three times. After each, the supernatant was discarded, and the bottom body redisperse in deionized water. A glass rod was used to homogenize large aggregates. Then, the suspension of chitin nanocrystals was dialyzed against distilled water for 72 h. The nanocrystalline aggregates were removed by filtration through N° 2 sintered plate funnel. The dispersion concentration was determined gravimetrically by drying the samples at 70 °C until a constant mass was obtained. The suspension was stored at 4 °C for posterior use.

3.9 Characterization of chitin nanocrystals

The chitin nanocrystals were characterized by FTIR, mean particle size and Zeta potential (ζ). The FTIR spectra of the samples were determined using a Fourier Transform Infrared Spectrometer (FTIR) (IR trace-100), between 4000 and 400 cm^{-1}. The zeta potential (ζ) of the CNC suspensions ($1x10^{-3}$ % w/v) was measured using a Nano ZetaSizer (Malvern, Model ZS 3600). Prior to determination, the samples were kept under stirring.

3.10 Preparation of hydrogels

Suspensions of chitin nanocrystals in concentrations ranging from 0.2 to 1.0% (w / v) were prepared by diluting the stock solution. The NSC was dissolved into nanocrystals suspension at 3% (w/v) concentration under stirring for 24 h at 50 °C. The OxGM was dissolved in distilled water (30 min, 50 °C) to prepare a 3% (w/v) solution. The solutions of OxGM and NSC + CNC were mixed in a ratio of 1:1 (v/v) in a 24-well plate. Hydrogels without CNC were prepared in a similar manner, except that the NSC was dissolved directly in distilled water. When necessary, the resulting hydrogels were frozen in ultrafreezer and then lyophilized for 48 h for further analysis. Table 1 shows the composition of the hydrogels produced.

Table 1 - Composition of hydrogels.

[a]OxGM (w/v %)	[b]NSC (w/v %)	[c]CNC (w/v)
3	3	0
3	3	0.20
3	3	0.40
3	3	0.60
3	3	0.80
3	3	1.00

[a]Oxidized galactomannan

[b] N-succinyl chitosan

[c]Chitin nanocrystals

3.11 Characterization of hydrogels

3.11.1 FTIR

The hydrogels were frozen in ultra-freezer and then lyophilized for 48 h. The hydrogels were powdered in a mortar with a little liquid N_2 and mixed with KBr to prepare the pellets. The FTIR spectra of the samples were determined using a Fourier Transform Infrared Spectrometer (FTIR) (IR trace-100) between 4000 and 400 cm^{-1}.

3.11.2 Porosity

The porosity of the hydrogels was measured by the liquid displacement method described by Sarker et al., 2016. Hydrogels prepared in 24-well plates were lyophilized, immersed in absolute ethanol, and centrifuged for 10 min at 1200 rpm to facilitate ethanol penetration because the hydrogels float in absolute ethanol. After centrifugation, excess ethanol from the surface of the hydrogels was removed with a filter paper and the hydrogel was weighted. The hydrogels were then held in ethanol and their weight measured at regular intervals until the weight became constant. At this time, it was assumed that the pores of the hydrogels were saturated with ethanol. The porosity of the hydrogels was calculated from the equation:

$$\text{Porosity } (\%) = (W_2 - W_1)/\rho V \text{ X } 100 \qquad (5)$$

where W_1 and W_2 are the weight of lyophilized hydrogels before and after immersion in absolute ethanol, respectively; ρ is the absolute ethanol density and V is the volume of the hydrogel.

3.11.3 Scanning electron microscopy

The porous structure of the hydrogels was examined by scanning electron microscopy. The hydrogels were prepared in a 96-well plate, allowed to cure for 48 h, frozen in ultra-cold and lyophilized at -40 ° C for 48 h to remove water from the internal structure. The lyophilized hydrogels were cut with a scalpel blade, placed on the stub, and coated with a thin layer of gold. The morphology of the hydrogels was visualized in a Quanta FEG FEI-450 equipment.

3.11.4 Swelling

The degree of swelling of the hydrogels was determined gravimetrically at room temperature. The hydrogels were prepared in 24-well plates, allowed to cure for 48 h and then weighed. Subsequently, they were immersed in PBS solution (pH = 7.4) and water, and at predetermined time intervals, were removed and weighed. The degree of swelling (DS) was calculated by equation 5:

$$DS = (Ws-Wd)/Wd \times 100\% \quad (6)$$

where Wd and Ws represent the weight of dry and swollen gels, respectively. The experiments were performed in triplicate.

3.11.5 In vitro injectability

The injectability assay was performed by mixing the two solutions (OxGM and NSC), with or without CNC, into a 1 mL syringe with a cannula 26G (0,45x13mm). The solutions were mixed by inverting the syringe and after 2 min were injected onto a Petri dish. Additionally, we analyzed the ability of precursors to fill spaces with different shapes.

3.11.6 Dynamic Mechanical Analysis

Hydrogels (average diameter = 9 mm, height = 18 mm) were prepared in 3 mL syringes and analyzed in DMA25 METRAVIB at 37 °C. The syringe nozzle was removed and the solutions (750 μL of OxGM + 750 μL of NSC with or without CNC) were pipetted into it and homogenized by aspiration and dispensing of the mixture several times. The hydrogels were allowed to stand for 48 h to ensure complete crosslinking process. The hydrogels were subjected to a uniaxial compression test up to 5% deformation (0.02 mm/s) from the initial

height. The compression modulus was calculated from the inclination in the linear region of the stress/strain curve. The assays were performed in triplicate.

3.11.7 Gelation time

The gelation time was determined rheologically through the intersection between the storage module (G') and the loss modulus (G"). The two solutions were added in the lower plate of the rheometer and the evolution of G' and G" was evaluated. The point at which G' and G" intersect (crossover) was defined as the time of gelling.

3.11.8 In vitro drug release assay

Bovine serum albumin (BSA) was incorporated into hydrogels (with and without nanocrystals) to investigate their release profile. The BSA was dissolved in the NSC solution with stirring for 24 h. Then, the OxGM and NSC + BSA solutions were mixed inside syringes (3 mL) to obtain cylindrical specimens. The hydrogels were left to rest for another 24 to ensure complete gelation. The phosphate buffered saline (PBS) was used as a release medium to simulate physiological conditions. For the release test the hydrogels were placed in 50 mL of PBS buffer and taken to an incubator (37 ° C, 100 rpm). Aliquots (3 mL) were removed from the medium at pre-established time intervals for reading on the UV-Vis and then this volume was replaced by another 3 mL of new buffer. The wavelength used to quantify the BSA was 280 nm. **Figure 9** presents calibration curve used to determine the amount of BSA released.

Figure 9 - Calibration curve used to determine BSA released

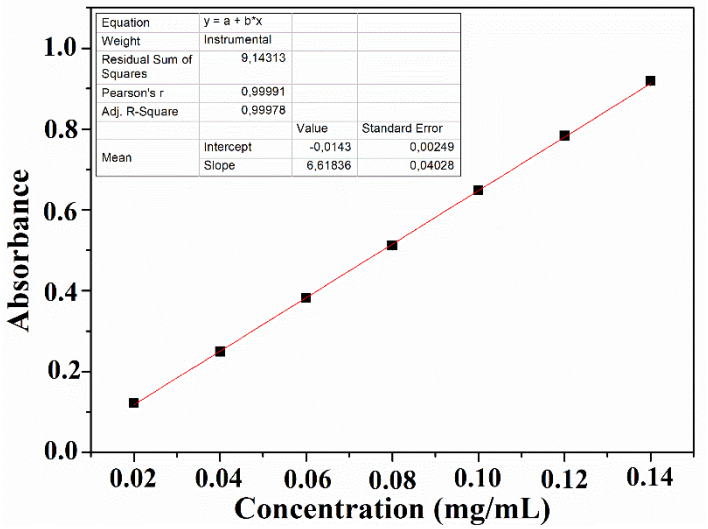

3.11.9 Cell viability

The cell viability was measured by the indirect method, where it evaluates the cytotoxicity through contact of the cells with the extracts obtained from the samples. To prepare

the extracts, initially, the hydrogels were cut to 1 cm in length and sterilized by UV radiation. The samples were then aseptically placed in 24-well plates, 1 mL of the supplemented DMEM culture medium (10% SFB and 1% penicillin/streptomycin) were added and incubated at 37 °C for 24 h according to the International Organization for Standardization, 10993-5 (2009). After the incubation period, the obtained extracts were collected and stored in Falcon tubes.

For the cell viability test, 100 µL of the L929 fibroblast cell media solution, with cell density of 6,000 cells/well, was seeded into 96-well plates. The plates were then incubated at 37 °C for 24 h. After this period, the cells adhere to the bottom of the well forming a cell monolayer. The cell solution was removed from the wells, added 100 µL of the extracts obtained from each sample and incubated at 37 °C for 24 h. After this time the extracts were removed from the wells and 150 µL of a 10% (v/v) solution of resazurin prepared in supplemented DMEM was added. This resazurin solution, commercially known as Alamar Blue, is widely used as an indicator of cell viability in many proliferation and cytotoxicity assays. The control group was made by exposing the L929 fibroblast cells only to the supplemented DMEM culture medium. Finally, the plates were incubated for 4 hours at 37 °C. This is the time required for the reduction of resazurin (blue/violet) to resorufin (fluorescent pink). After this period, 100 µL of each well was homogenized, collected and transferred to a new 96-well plate, where fluorescence readings were performed with 560 nm excitation and emission at 590 nm in a BioRad Model 540 ELISA spectrophotometer. Percentage of viable cells was calculated using the equation 7. The viability of the cells of the control group was adjusted to 100% for the calculation of mean values and standard deviation.

$$\textit{Cell viability}\,(\%) = (F\ \textit{sample} / F\ \textit{control group}) \times 100 \quad (7)$$

Where:

F sample - Fluorescence corresponding to a well containing sample;

F control group - Fluorescence corresponding to a well containing cells exposed only to the DMEM culture medium supplemented.

4 RESULTS AND DISCUSSION

4.1 Characterization of UnGM and OxGM

Periodate oxidation is a well-established procedure toward preparation of dialdehyde polysaccharides. These derivatives are commonly used to biomedical applications acting as crosslinking agent to proteins (collagen, gelatin, silk), synthetic or natural polymers functionalized with amine group (hydrazide-functionalized poly(N-isopropylacrylamide-*co*-acrylic acid), carboxymethyl cellulose-*g*-adipic dihydrazide) and natural occurring aminated polysaccharides (chitosan and partially deacetylated chitin) (SARKER et al., 2016; PATENAUDE and HOARE, 2012; WEI et al., 2015). Among the biomaterials produced using dialdehyde polysaccharides as a precursor there are sponges, wound dressing, preformed hydrogels, bioink for 3D bioprinting, microcapsules, films among others (REAKASAME and BOCCACCINI., 2018).

There is still a very small number of papers researching the use of dialdehyde prepared from galactomannan to produce injectable hydrogels. To better understand how and what is the role of dialdehyde galactomannan in the process of gelification we chosen it as the crosslinking agent.

During the oxidation with sodium periodate, the carbon-carbon bond between adjacent hydroxyl groups is cleaved opening the monosaccharide ring to get the dialdehyde derivative (**Figure 10**). Consequently, the backbone of the polysaccharide can move more freely in solution, thanks to a greater degree of freedom of rotation (GOMEZ; RINAUDO; VILLAR, 2007). The position of aldehyde groups varies according to the pattern of linkage of the units that form the polysaccharide. In the case of galactomannan, only the secondary hydroxyl groups are converted to aldehyde (C2, C4 of galactose unit and C2, C3 of mannose unit). Carbon at the C3 position in galactose is expelled as acid formic leading to decrease in the pH solution. As the hydroxyl present in C6 (in galactose and the non-substituted mannose units) is primary, it cannot be oxidized by sodium periodate, but in the presence of TEMPO (2,2,6,6-Tetramethyl-1-piperidinyloxy) it can be oxidized to carboxyl groups.

Figure 10 - Representation of oxidation reaction of galactomannan. The arrows (⟶) indicate the bonds cleaved to form the aldehyde groups

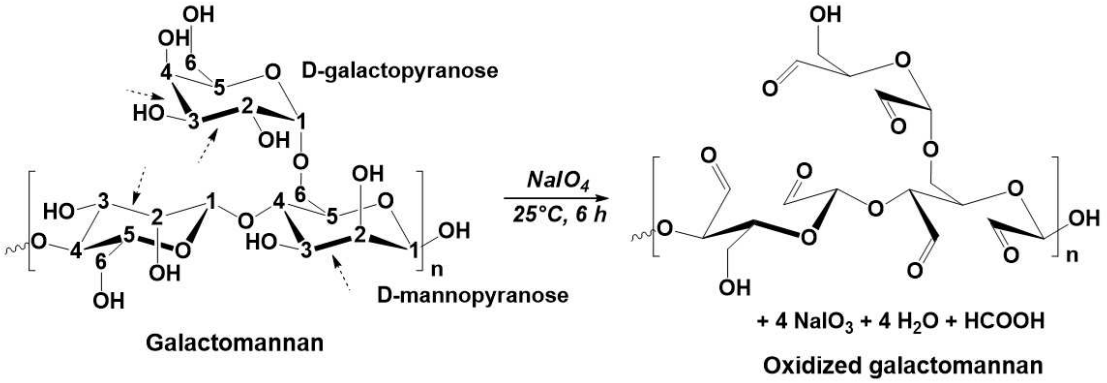

The mechanism for this reaction involves the formation of a 5-membered intermediate cyclic iodate ester (step 4 in **Figure 11**) followed by simultaneous binding cleavage to generate aldehyde groups (step 5 in **Figure 11**) (VARGHESE et al., 2013). Structural characteristics that retard the rate of formation of the cyclic intermediate slow down the reaction (CAREY; SUNDBERG, 2007). Therefore, to occur oxidation of vicinal diols, the OH groups must be oriented in an equatorial-equatorial or axial-equatorial position. Vicinal OH groups in a rigid trans-diaxial position cannot react with the ion periodate, because formation of the intermediate complex is hindered by the far distance between the OH groups (KRISTIANSEN; POTTHAST; CHRISTENSEN, 2010).

Figure 11 - Mechanism of the oxidation reaction between a unit of galactose and sodium periodate

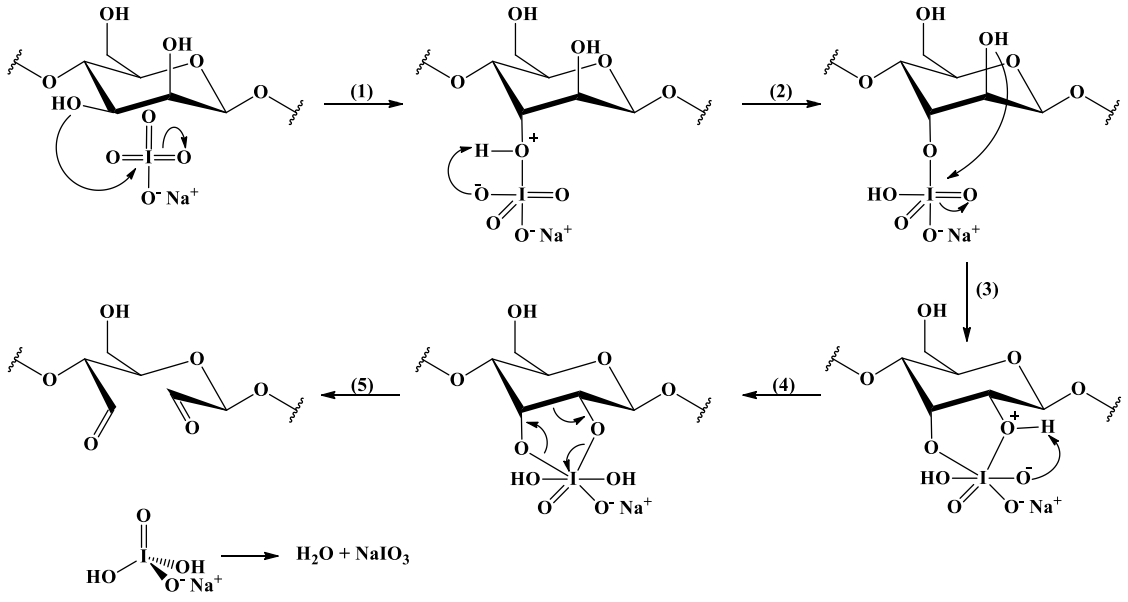

After the oxidation reaction, OxGM showed a decrease in its solubility in water and PBS. We hypothesize that is due to the decrease of the hydroxyl content over the backbone (number of hydroxyl before/after the oxidation = unsubstituted mannose: 3/1; mannose substituted: 2/0), which resulted in a lower hydrophilicity. During the reaction, -OH are converted to -CHO and this groups does not interact so well with water. While the OH can interact by hydrogen bond and dipole-dipole, the -CHO use only dipole-dipole force.

The degree of oxidation was defined as the number of units modified per 100 monosaccharide units and considering two aldehyde groups per unit modified. There are some methods described in the literature for determining the degree of oxidation, but two of them are more relevant: complex formation with tert-butyl carbazate followed by hydrogen NMR analysis and a titration method that employs hydroxylamine hydrochloride. The titration method involves a nucleophilic attack of the hydroxylamine nitrogen to the carbonyl carbon of oxidized derivatives leading to the formation of a polyoxime derivative (C=N-OH) with the release of one molecule of water and other of HCl. The degree of oxidation determined based on titration curve was 40.3%. This value is slightly lower than the theoretical value (50 %), that can be explained by the incomplete consumption of $NaIO_4$. In general, this decrease is common and has been reported in several studies involving oxidized polysaccharides (AMER et al., 2016).

FTIR was carried out to confirm the oxidation performed by sodium periodate (**Figure 12**). As expected, there is not too many differences between the spectra. This is a widely well-known characteristic for dialdehyde polysaccharides. It is possible to verify the appearance of a band at 1723 cm^{-1}, related to C=O symmetric vibration of aldehyde in free form, an indicative of the functionalization of GM. One justification that may explain the low intensity of the free aldehyde band is to the formation of different equilibrium structures, among which are hemiacetals (MAIA et al., 2005; ZHANG et al., 2017) (**Figure 13**). These structures decrease the content of carbonyl and mask your sign. The band at 875 cm^{-1} can be correlated to the C–O–C bridges from hemiacetals (MÜNSTER et al., 2017).

Figure 12 - FTIR spectrum of unmodified galactomannan and oxidized galactomannan

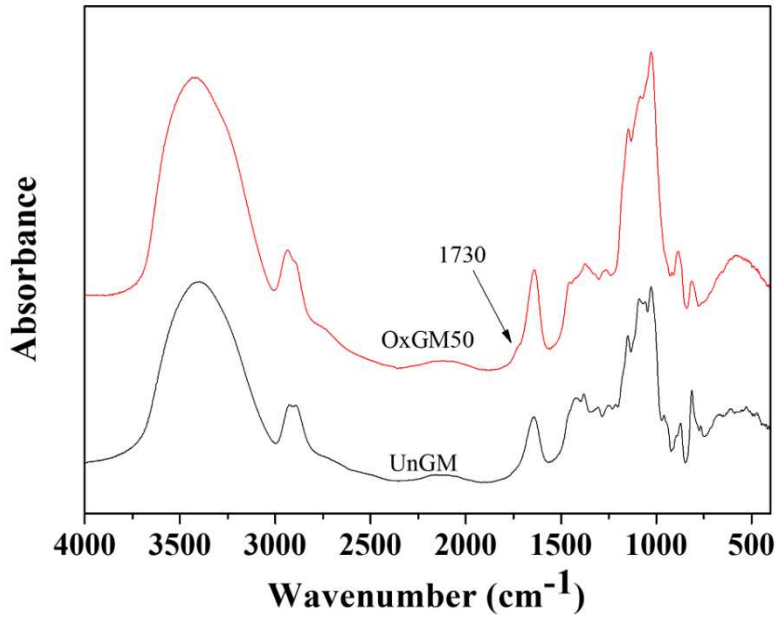

Figure 13 - Structural possibilities for the glycosidic units of the oxidized galactomannan. (I) free aldehyde, (II) intramolecular hemiacetal, (III) hemialdal, (IV) hydrated aldehydes and (V) intermolecular hemiacetal

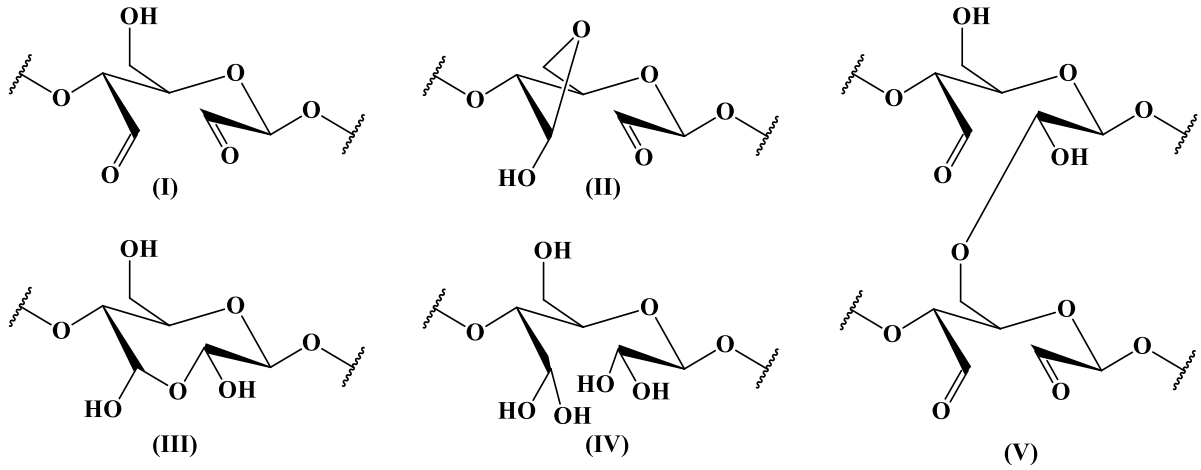

Source: Adapted from Sirviö et al., 2014 and Plappert et al, 2018.

GPC analysis was performed to understand the effect of the oxidation reaction on the GM chain. In **Figure 14** is possible to see a band shift of the oxidized derivative to a higher elution volume as compared to the UnGM. This increase is indicative of the decrease in the peak molar mass. The oxidation reaction led to the breakdown of some glycosidic bonds.

Polysaccharides in the dialdehyde form are hydrolyzed more easily than the unmodified and small amounts of acid can cleave the β-(1→4) glycosidic linkage between the units. This type of observation is common for dialdehyde polysaccharides (AMER et al., 2016).

Figure 14 - Chromatogram of unmodified galactomannan and oxidized galactomannan

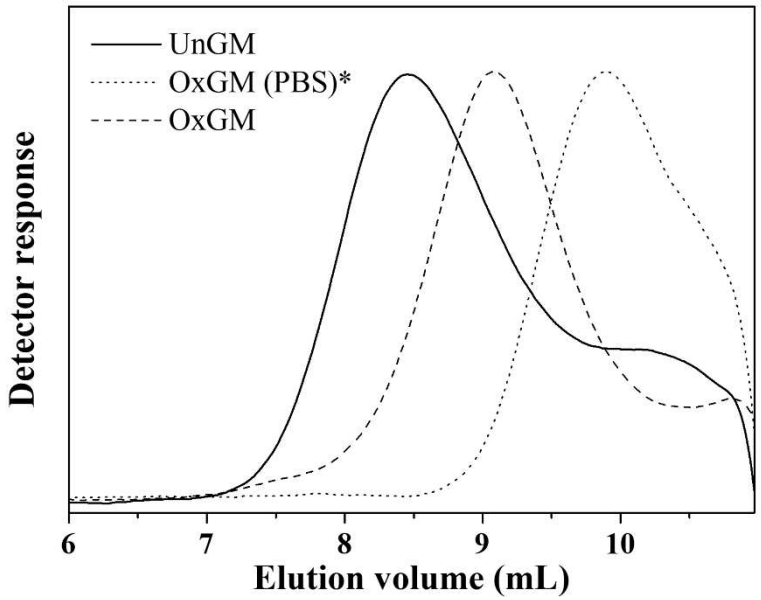

Figure 15a shows the ^{1}H NMR spectrum for *Delonix regia* unmodified galactomannan. In the anomeric region two distinct signals are observed. The signal at 5.02 ppm corresponds to the H-1 of the α-D-galactopyranose ring, and the signal at 4.73 ppm corresponds to the H-1 of the β-D-mannopyranose ring. The mannose/galactose ratio was obtained by integrating these areas, obtaining a value of 2.7.

Figure 15 - 1H NMR spectrum of a) unmodified galactomannan and b) oxidized galactomannan

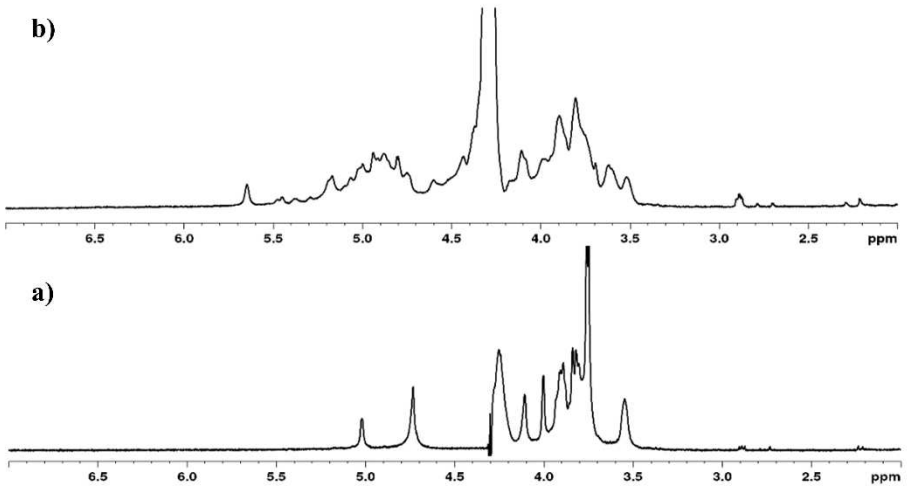

With the oxidation it is possible to observe the appearance of a 5.6 ppm peak that can be attributed to hemiacetal formation (**Figure 15b**). The appearance of new peaks between 4.5 and 5.6 ppm is also related to the formation of different hemiacetallic structures (MAIA et al., 2005).

4.2 Characterization of CT and NSC

The graft of chitosan with acrylic monomers (QU et al., 2017), quaternization (Ren et al., 2017) and acylation (HUANG et al., 2016) are proposed in literature as an alternative to improve the solubility of chitosan in aqueous medium. Here we utilized the succinylation. N-succinyl chitosan (NSC) was obtained via ring-opening reaction with succinic anhydride in homogeneous environment.

The derivative NSC have been applied to various biomedicals fields such as encapsulation of drugs (XING et al., 2019), prevention of postoperative peritoneal adhesions (MITSUHASHI et al., 2019), drug release (BASHIR et al.,2017).

This reaction takes places by a nucleophilic attack of primary amine from glucosamine unit of chitosan to carbonyl carbon of the succinic anhydride (interaction HOMO→LUMO). As oxygen from hydroxyl groups have nucleophilic character, the O-substituted derivative also can be formed. Nevertheless, we believed that the N-substituted derivative is preferentially produced, because the electrons from nitrogen are more available than the oxygen. After processed the reaction, pH wad adjusted to precipitate the NSC and obtain it in salt form (COO^-Na^+) that interact more strongly with water. The **Figure 16** shows a representation of the reaction.

Figure 16 - Succinylation reaction between glucosamine unit of chitosan and succinic anhydride

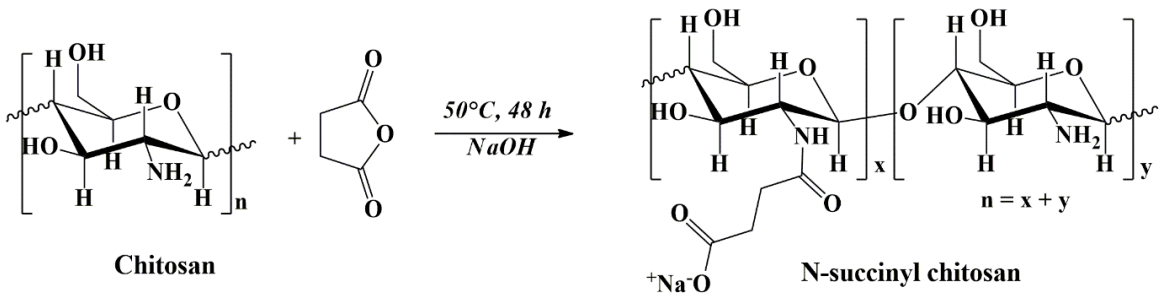

We performed a qualitative test to try to understand the effect of the modification on the macroscopic properties of the derivative. From **Figure 17**, the macroscopic appearance of the NSC solution can be compared to unmodified chitosan (both 3.0% w/v) at different pH values. It is possible to verify that the modification was efficient in increasing the pH range at which the derivative can be solubilized (pH = 5.5 - 13), whereas unmodified chitosan was soluble in acid pH (pH = 3). This happens due to the presence of the carboxylate groups that act both to stabilize the solution through electrostatic repulsions and to increase the hydrophilicity of the derivative by establishing hydrogen bonds.

Figure 17 - Macroscopic aspect of the solutions of a) chitosan and b) N-succinyl chitosan (3% w/v) at different pH values (pHs: 3, 5.5, 7.4 and 13)

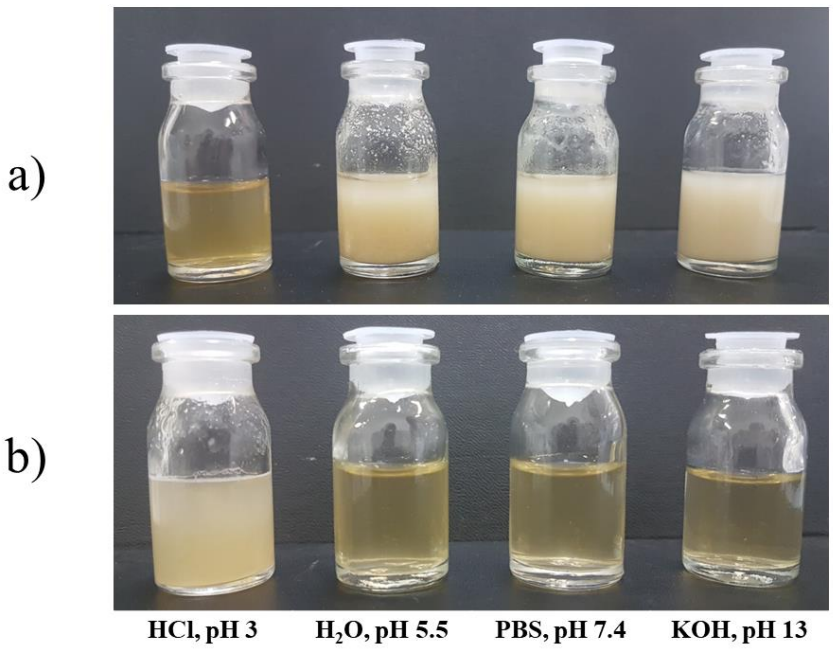

Analysis of FTIR was made to evaluate the effect of graft of succinic anhydride onto the structure of chitosan (**Figure 18**). In the spectrum of chitosan, characteristic bands of amide I at 1656 cm^{-1} (C=O stretching) and amide II at 1597 ($-NH_2$ bending) are observed. The bands at 2919 and 2876 cm^{-1} are assigned to asymmetric and symmetric stretching of C-H, respectively. Typical bands of polysaccharide are observed at 1155 cm^{-1} (C-O-C stretching), 1075 and 1033 cm^{-1} (both related to vibration involving C-O stretching). After modification, a slight increase in intensity of the band referent to stretching of C-H was observed, probably due to the insertion of the methylene groups of the succinic anhydride (–NH – CO – **CH_2** – **CH_2** – COO^-). Also, it is verified a strong increase in the amide I band absorbance, caused by the

presence of COO^- group from succinic anhydride. The new band at 1400 cm^{-1}, is attributed to symmetrical stretching of COO^- succinyl group. The absence of a band in the range 1710-1760 cm^{-1}, which refers to the signal of O-acyl ester groups, indicates that the succinyl group was highly selective to the amide group of glucosamine unit (BASHIR et al., 2017; LIN et al., 2011).

Figure 18 - FTIR spectrum of chitosan and N-succinyl chitosan

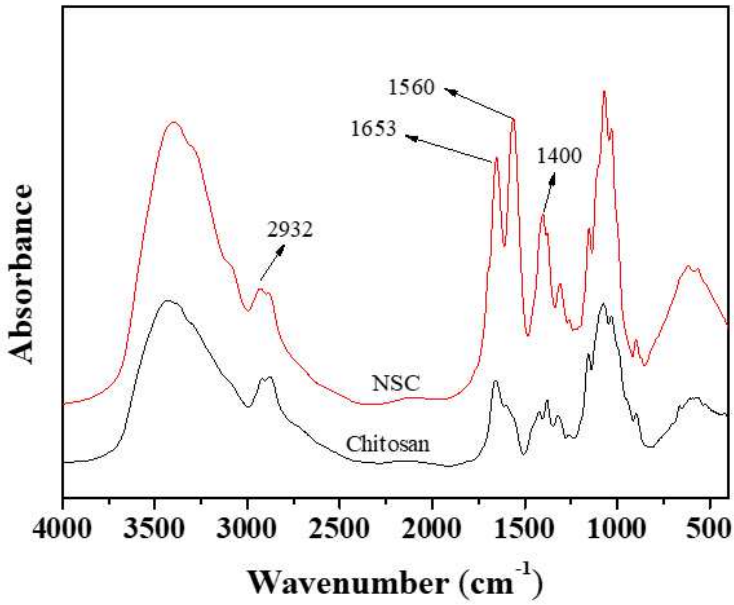

The **Figure 19a** and **Figure 19b** present NMR spectra for chitosan and NSC. The chitosan has signals at chemical shifts of 2.01 ppm, that are corresponding to protons of the acetyl group from the acetylated unit.

Figure 19 - ^1H NMR spectrum of a) chitosan and b) N-succinyl chitosan

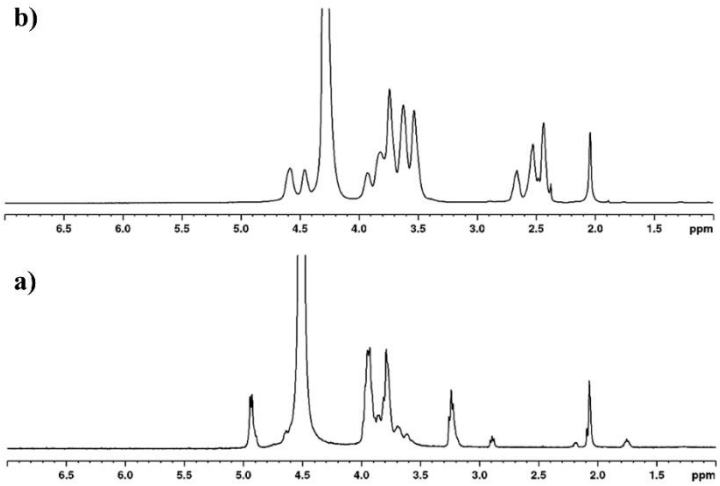

The peak at 3.2 ppm is related to the anomeric protons of glucosamine unit, and the signals in the region of 3.4 to 4.0 ppm are assigned to the non-anomeric protons of the chitosan backbone (TANG et al, 2016). After the reaction we can see new signals in the region between 2.4-2.6 that can be assigned to the methylene groups (–NH – CO – **CH_2** – **CH_2** – COO^-) of succinic anhydrides.

4.3 Characterization of chitin and CNC

Chitin is a semi crystalline polysaccharide where the chains are organized in sheets that are strongly held together by intra- and intermolecular hydrogen bonds between adjacent saccharide units (RINAUDO, 2006). Chitin flakes were hydrolyzed with a concentrated acid solution to remove amorphous region and isolate the nanocrystals as water-insoluble rod-like particles (**Figure 20**). Disordered domains are dissolved in the acid because they are more susceptible to hydrolysis and domains of high crystallinity continue intact in solution (ZENG et al., 2012). The suspension of chitin nanocrystals had a milky appearance (**Figure 21**).

Figure 20 - Schematic representation of the obtaining process of the chitin nanocrystals from chitin flakes

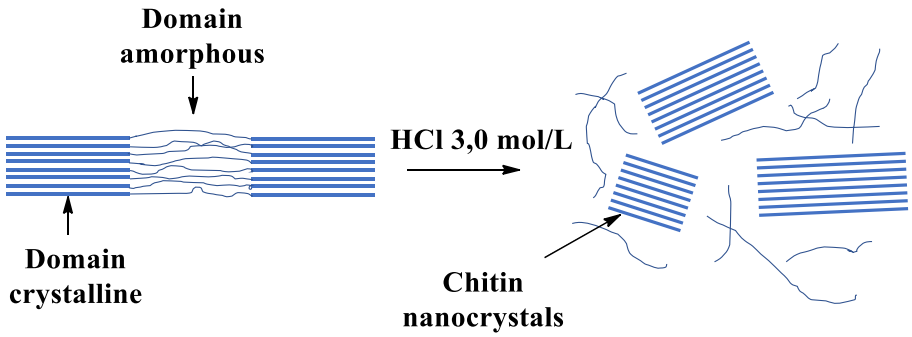

Figure 21 - Aspect of chitin nanocrystal suspension

The analyses of Zeta potential ($\zeta = + 55.9 \pm 10$ mV) shows that the suspension has positive charge when in water. This behavior is due to the protonation of primary amino groups on the surface of nanocrystals to give $-NH_3^+$. The NH_2 group was probably generated by deacetylation during the purification step. These positive charges contribute for stabilization of the suspension by electrostatic repulsion among the charged particles. This effect also is observed when cellulose nanocrystals are extracted from some cellulosic source. However, in the case of cellulose the charges are negative due the H_2SO_4 used that attach some $-SO_3^-$ groups on surface of the crystals. The high value of the zeta potential (in module), led to the more stable suspension and prevents aggregation of nanoparticles.

FTIR spectra of the chitin powder and CNC are displayed in **Figure 22**. In CNC spectrum we can bands related to amide I (stretching C=O, at 1661 and 1622 cm^{-1}), amide II (stretching C-N combined C-N-H bend, at 1558 cm^{-1}) and amide III (stretching C-N combined C-N-H bend, at 1314) (LI et al., 2018). After inspecting the spectrum, it is possible to verify that it still presents bands characteristic of an α -chitin. The CNC has more sharp bands as result of high crystallinity.

Figure 22 - FTIR of chitin powder and CNC

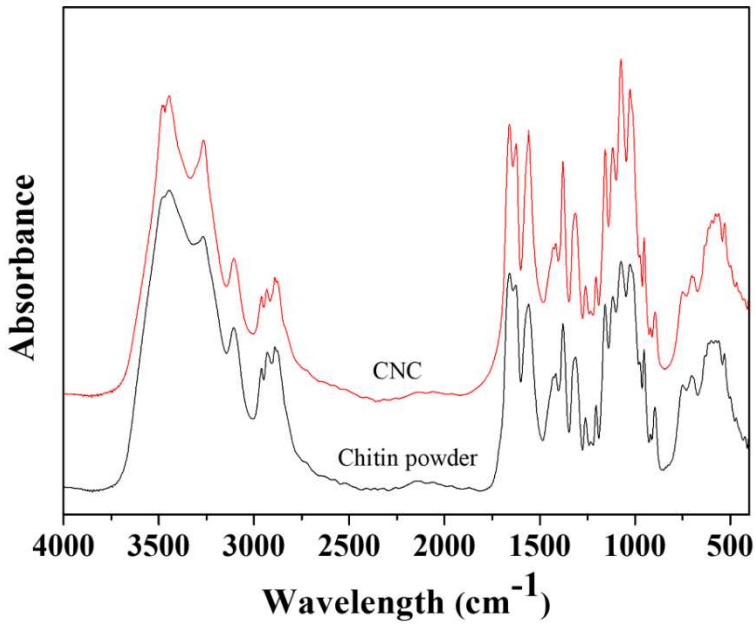

In **Figure 23** it is possible to observe the size distribution of CNCs in water. There are two distinct populations, the majority being 444 nm in size. It is noteworthy that the size determination made by DLS considers the particles as spherical and uses the hydrodynamic

radius of the particle. This causes deviations between measured and real value because hydration water molecules can make the material larger than it actually are.

Figure 23 - Distribution of the particle size of the chitin nanocrystals

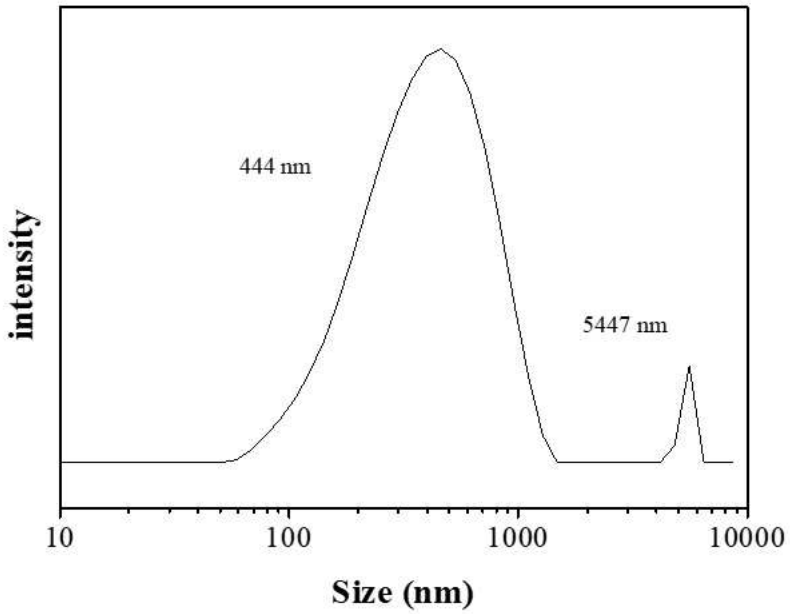

From the AFM analysis it was possible to determine the morphology and size of CNCs. Generally, the process to obtain the chitin, with at least one dimension on the nanometer scale, is made by using high-pressure homogenization (microfluidization), strong inorganic acids or by selective oxidation of primary alcohol groups in the presence of 2,2,6,6-tetramethylpiperidine-1-oxyl (TEMPO) radical followed by mechanical disintegration (YANG et al., 2020). Between these, the more common and widely used is that apply solutions of strong inorganic acid, like HCl or H_2SO_4, which removes the amorphous domain (deacetylated units). The crystalline domain is isolated at nanoscale and is generally known as nanocrystal, nanowhiskers or just as whisker (ZENG et al., 2012).

It is important to differentiate between nanocrystals and nanofibers. While to produce nanofibers are generally applied physical methods to disintegrate fibers, like ultrasonication, microfluidization or high-speed blending, nanocrystals pass through a chemical harsh process that consumes regions of high disorder (amorphous domain) and highly organized regions (crystalline domain) are isolated on the nanometric scale (LARBI et al., 2018; JIN et al., 2021). This differentiation is valid for both cellulose and chitin.

In terms of shape and size, nanocrystals are described as stretched structures in which the width it is smaller than length, generally in nanoscale. The dimensions of nanocrystals vary greatly according to the acid concentration and reaction time used in their extraction. In case of nanofibers the width is nanoscale, and the length is much higher, usually reaching micron size (JIN et al., 2021) (**Figure 24**). The morphology was predominantly rod-shaped with a uniform distribution with length 789 ± 0.07 nm and diameter 237 ± 0.04 nm. This is equivalent to an aspect ratio of about 3.3. The shape observed is like that described in the literature (ZENG., 2012). It is noteworthy that the morphology can vary greatly based on the method and extraction conditions used.

Generally, the process to obtain the chitin, with at least one dimension on the nanometer scale, is made by using high-pressure homogenization (microfluidization), strong inorganic acids or by selective oxidation of primary alcohol groups in the presence of 2,2,6,6-tetramethylpiperidine-1-oxyl (TEMPO) radical followed by mechanical disintegration (YANG et al., 2020). Between these, the more common and widely used is that apply solutions of strong inorganic acid, like HCl or H_2SO_4, which removes the amorphous domain (deacetylated units). The crystalline domain is isolated at nanoscale and is generally known as nanocrystal, nanowhiskers or just as whisker (ZENG et al., 2012).

It is important to differentiate between nanocrystals and nanofibers. While to produce nanofibers are generally applied physical methods to disintegrate fibers, like ultrasonication, microfluidization or high-speed blending, nanocrystals pass through a chemical harsh process that consumes regions of high disorder (amorphous domain) and highly organized regions (crystalline domain) are isolated on the nanometric scale (LARBI et al., 2018; JIN et al., 2021). This differentiation is valid for both cellulose and chitin.

In terms of shape and size, nanocrystals are described as stretched structures in which the width it is smaller than length, generally in nanoscale. The dimensions of nanocrystals vary greatly according to the acid concentration and reaction time used in their extraction. In case of nanofibers the width is nanoscale, and the length is much higher, usually reaching micron size (JIN et al., 2021).

Figure 24 – AFM for chitin nanocrystals

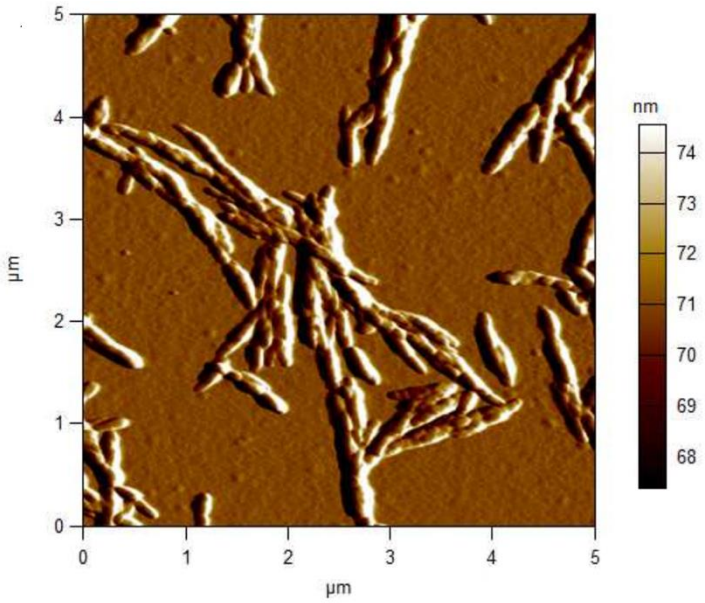

Figure 25 shows the CNC suspension between polarized light filters. This experiment aims to visualize the birefringent character of the suspension. In the first image we have the suspension without shaking and then under the effect of it. Birefringence can be considered as a criterion to determine the anisotropic nature of a particular material, in addition to being a strong indicator of good dispersibility and the presence of nanocrystals in solution.

Figure 25 - Birefringence of nanocrystal suspension a) without and b) under shaking

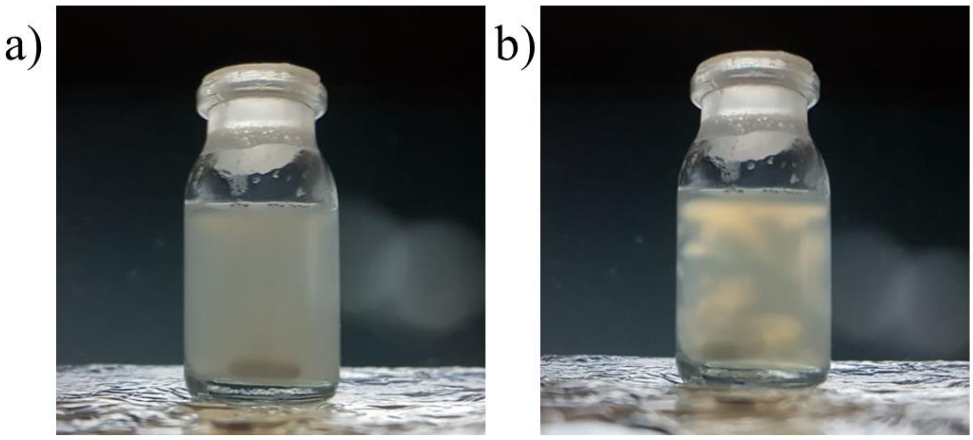

The CNC suspension has some viscosity associated that increase with the concentration. The same effect can be observed for nanocrystals and nanofibers prepared from cellulose. **Figure 26** show the effect of three different concentrations over the viscosity of CNC. The viscosity in 3% suspension is almost twice that presented in 1%. This effect is due to the sum of the forces of the hydrogen bonds between the hydroxyl groups present on the surfaces

of the nanocrystals. In fact, suspensions of nanocrystals and nanofibers in concentration upper 10-15% w/v present a semi-solid like (LIU et al., 2018b).

Figure 26 - Effect of concentration over the dispersion of chitin nanocrystals

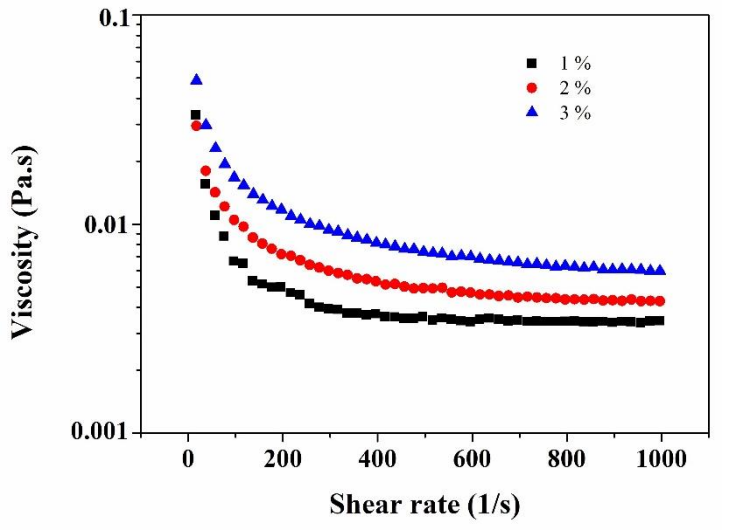

In the **Figure 27** is possible see how the presence of different percentage of CNC affected the viscosity of NSC solution. As demonstrated, the higher the percentage of CNC present in the NSC solution, the higher the viscosity observed. In fact, to CNC 0.8 and 1.0% suspension they formed a solution that had a like gel aspect. Despite the increase in viscosity the solutions were fluid and could be pipetted to prepare the hydrogels.

A low viscosity of the precursor solutions can facilitate the use of the hydrogel for a greater number of potential clinical applications since it can be administered with a high caliber like 18 G or even smaller caliber like 33 G (PATENAUDE, SMEETS and HOARE., 2014).

Figure 27 - Effect of CNC concentration over viscosity of the N-succinyl chitosan

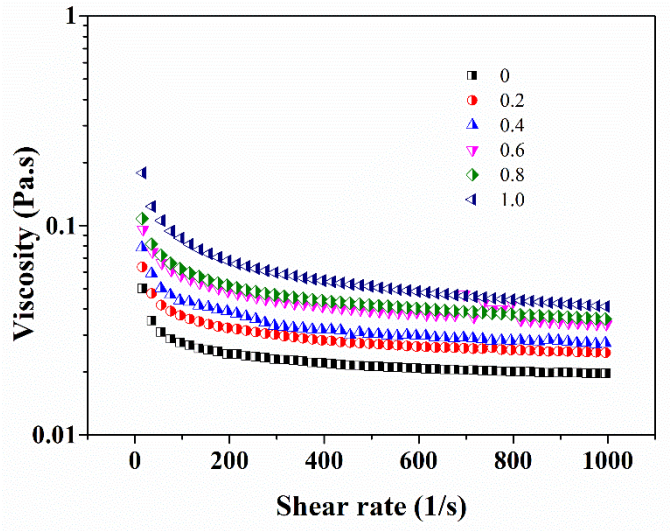

4.4 Characterization of the hydrogels

Hydrogels were prepared by the combination of OxGM + NSC or OxGM + (NSC + CNC) solutions. As is known, injectable hydrogels based only in soluble natural polymers suffers with the lack of stiffness. The incorporation of rigid organic nanoparticles, chitin nanocrystals, into hydrogel matrix was a manner to try improving the mechanical properties by creation of a composite material. The choice of chitin nanocrystals lies in their biocompatible properties, renewable nature, and mainly by the fact that are only few papers that report utilization of nanocrystals as reinforcement agent to injectable hydrogels (DE FRANCE et al., 2016; LIU et al., 2018; SILVA et al., 2018; WANG; CHEN; CHEN, 2017), with the majority of papers using cellulose nanocrystals and not chitin.

As mentioned before, there are a great variety of ways of how two or more polymers can be combined to produce a biomaterial. Nevertheless, a quick search in literature reveal that Schiff base reaction is probably the most widely used approach to induce the chemical crosslinking in injectable hydrogel. Although there is a wide range of options available, schiff-based crosslinking is generally chosen due the mild reaction conditions, to be processed at room temperature and to takes place in non-organics solvents.

4.4.1 Macroscopic characteristics of hydrogels and gelation mechanism

In **Figure 28**, is verified the difference in tonality in the hydrogels without and with the presence of CNCs prepared in a 24-well plate. The hydrogel without CNCs showed a slight yellowish coloration due to the solution of chitosan and formation of Schiff bases. In the other hydrogels, this visualization is hampered by the presence of CNCs. It is possible to observe still that with the increase of CNC percentage in the hydrogels there was a change of coloration of slightly yellowish to opaque white. This increase in opacity is not an unexpected behavior since the CNC suspensions themselves became less and less translucent as their concentration increased.

Figure 28 - Macroscopic aspect of NSC-OxGM hydrogel with different concentrations of CNC

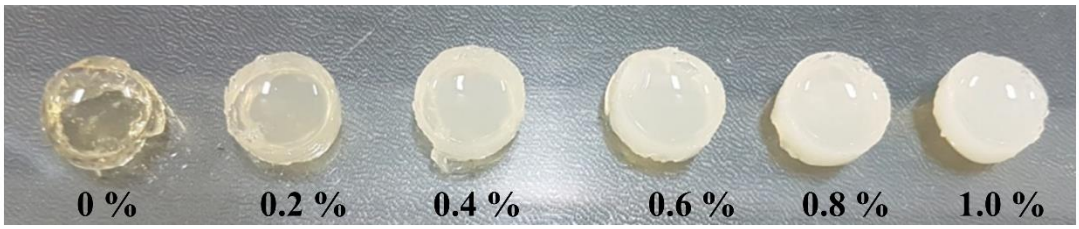

The transparency of structures reinforced with polysaccharide nanocrystals (cellulose and chitin) depends basically on the amount of filler added (concentration) and the thickness of the material in question (SHEN et al., 2016). For example, PLAPPERT et al., 2018, produced dialdehyde cellulose films, reinforced with 7.2% (w/v) cellulose nanocrystals, with a thickness of ~ 100 µm, which exhibited 90% light transmittance. Already HUANG et al., 2015, working with sodium alginate hydrogels reticulated with $CaCl_2$ and reinforced with chitin nanocrystals, obtained increasingly opaque hydrogels as the percentage of nanocrystals increased.

Regardless of the color change, the reinforced hydrogels obtained in this work appeared to have a homogeneous distribution, with no evident aggregation point of CNCs. It is noteworthy that as the CNC content increased, the hydrogels became visibly stronger, which could be translated by their ease of handling (**Figure 29**).

Figure 29 - Macroscopic aspect of the NSC-OxGM hydrogel containing 1% CNC

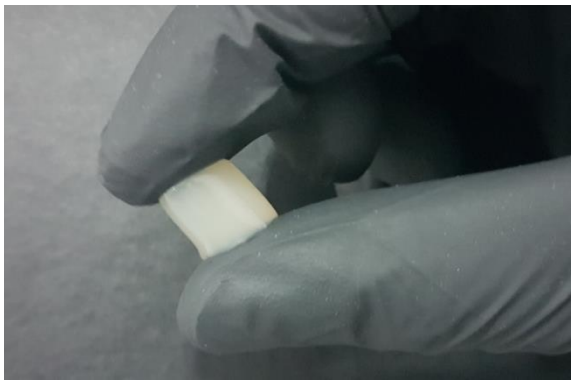

Formation of the hydrogel network, in other words, the gelling mechanism, from the precursor solution involves the development of cross-links between the aldehyde groups from OxGM and the remaining amine groups from NSC (not all amine groups are substituted by succinic anhydride), leading to formation of Schiff base (-C=N-) (**Figure 30**). Since CNCs do not have groups that can chemically interact with the matrix, we imagine that they were physically trapped and dispersed throughout the whole matrix, probably by establishing hydrogen bonds with the hydroxyl groups of the adjacent chains, acting as a filler to create a more resilient material.

Figure 30 - Reaction scheme showing the crosslinking process of the hydrogels

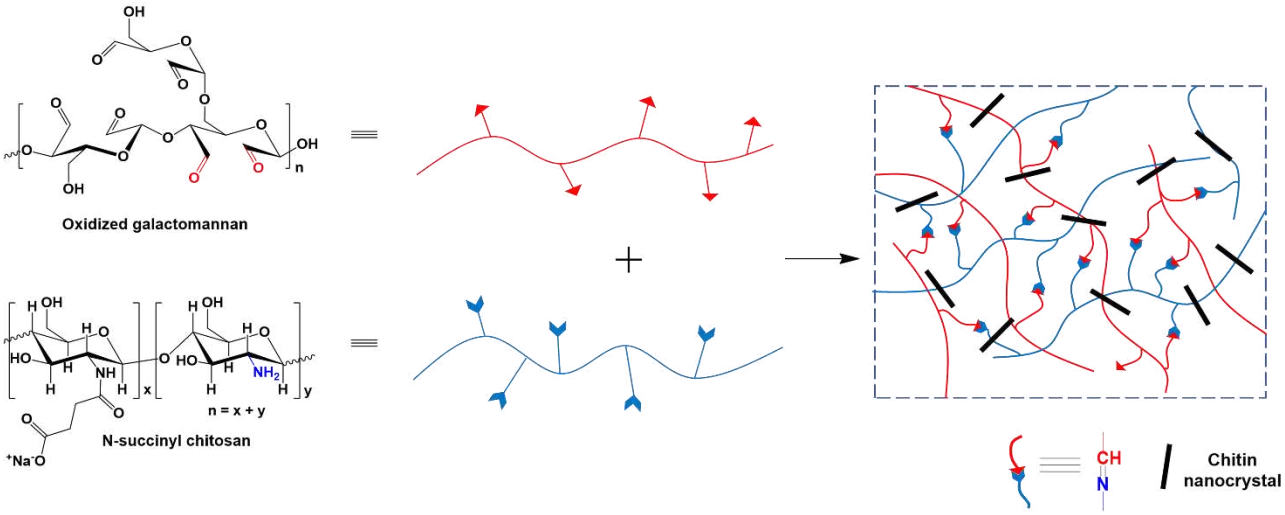

The formation of Schiff base reaction is based on a six-step mechanism where the first three steps lead to formation of an intermediate know as carbinolamine and in the three next steps occur the conversion of carbinolamine to an imine as the final product (**Figure 31**). The first step led to protonation of the carbonyl compound that increase it electrophilic character. Following, a primary amine act as a nucleophile and attack the carbonyl carbon

forming a tetrahedral intermediate. The previous intermediate is deprotonated to form the carbinolamine. Then the OH group is protonated converting it into a good leaving group. Simultaneously, the exit of a water molecule is formed a double bond C=N. The last stage involves the deprotonation of the intermediate with the subsequent formation of the imine (KLEIN, 2016).

Figure 31 - Mechanism involved during the formation of Schiff base between a primary amine and carbonyl compound that can be either an aldehyde or a ketone

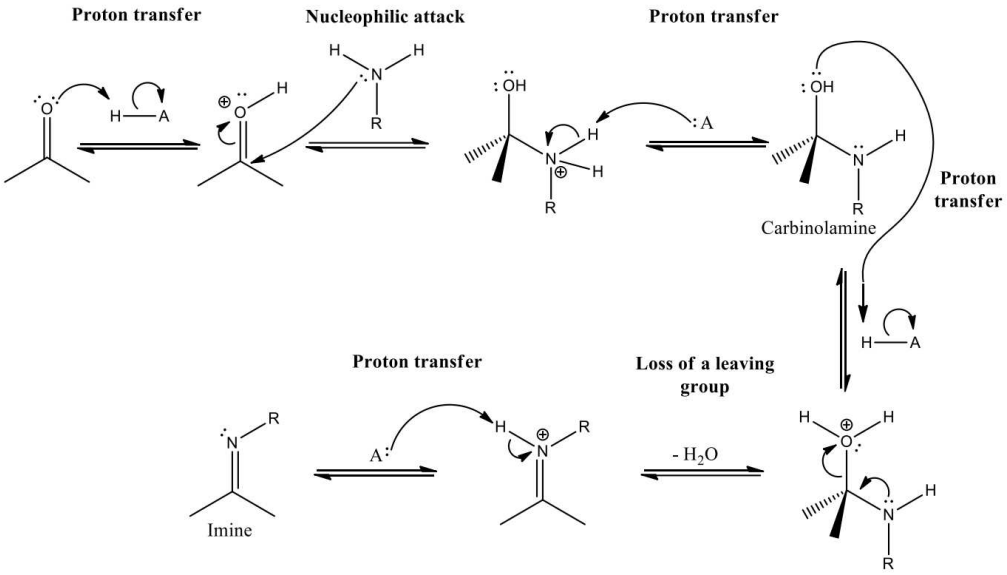

4.4.2 FTIR

Figure 32 presented the FTIR spectrum of the hydrogels compared to CNC. As the difference in term of CNC percentage between the hydrogels is low, all the spectras present very similar bands, with few differences between them. It is possible see that hydrogels have characteristics band of CNC and NSC at 1658 and 1561 cm^{-1}, respectively. It is possible to see the higher the percentage of CNC in the hydrogel, the greater the degree of similarity with the spectrum of the nanocrystals with the sharpest bands between 1000 and 1500 cm^{-1}. It is still possible to verify a band at 3270 cm^{-1}, associated with the N-H stretching that is more prominent for the gels with higher CNC content. This indicates the incorporation of fillers in the matrix of hydrogel. It is not possible to see the band referring to the Schiff base, indicative of the reticulation reaction. This is because it is in the region of 1665 cm^{-1} and so it is masked by the presence of other bands.

Figure 32 - FTIR spectrum of hydrogels with and without the addition of chitin nanocrystals

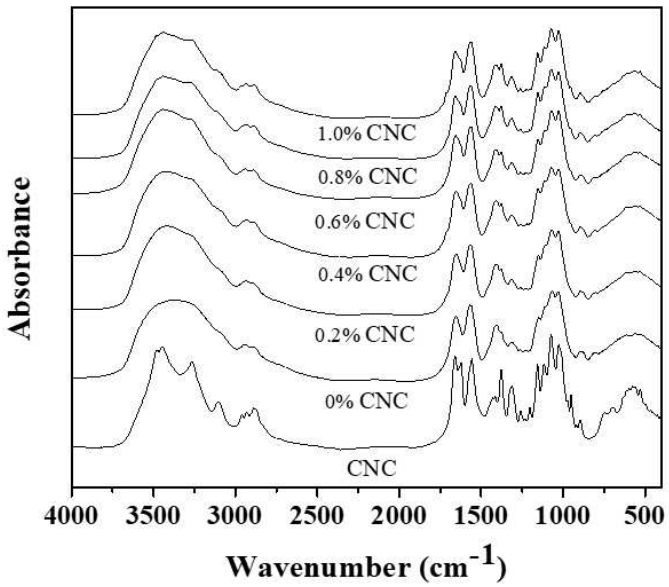

4.4.3 Porosity

According to KARAGEORGIOU and KAPLAN, 2005, porosity is defined as the percentage of empty space in a solid. It is of fundamental importance in the design of biomaterials for cell culture, since highly interconnected and highly organized porous networks facilitate the transit of nutrients, gases and components secreted by cells (MATHEW et al., 2018). It was possible to observe that all the hydrogels produced, regardless of the CNC content, had low values of porosity, between 60 and 77% (**Figure 33**). There does not seem to be a direct correlation between the percentage of CNC and the degree of porosity observed. These relatively low values are important for maintaining the hydrogel structure since porosity is closely related to mechanical properties. Stiffness decreases as porosity increases (ANNABI et al., 2010).

Figure 33 - Percentage of porosity of hydrogels with different CNC contents

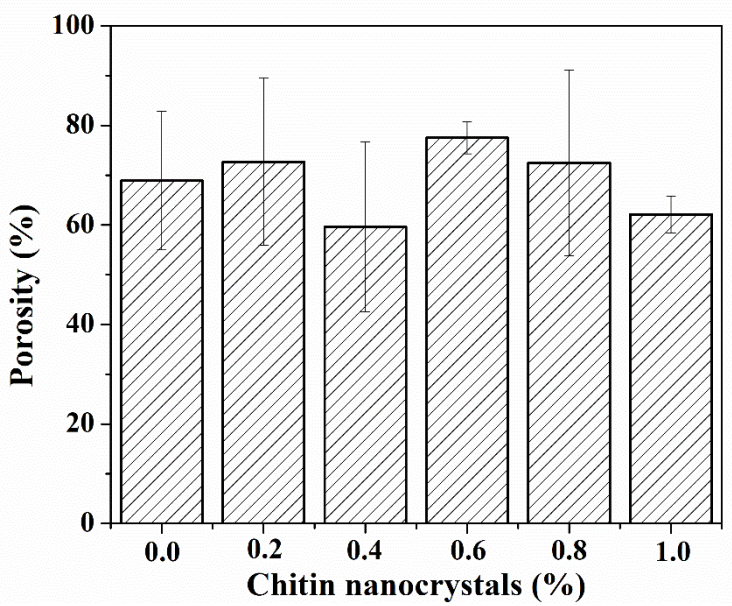

The porous structure of the hydrogels was formed due to the freeze-drying process which consists of freezing, whereas the ice crystals are formed the solute molecules (such as polymer molecules, nanoparticles) are expelled to the boundaries between the crystals of adjacent ice. In the lyophilization step, or drying under high vacuum, the solvent molecules are sublimated giving rise to void spaces, the pores (HEIMBUCK et al., 2019; YANG et al., 2017) (**Figure 34**). The water acted as a "template" for the channels that gave rise to the pores.

Figure 34 - Scheme showing the process of exclusion of solute molecules during freezing

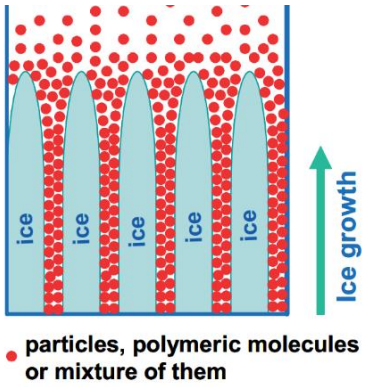

Source: ZHANG and COOPER, 2007.

4.4.4 Scanning Electron Microscopy

The internal morphology of hydrogels and the influence of the introduction of CNCs on their structure was evaluated by SEM. Although the freezing-drying technique does

not reliably translate the structure of hydrogels while hydrated, we can have a sense of its microstructure. **Figure 35** shows the SEM for gels with 0, 0.4 and 1.0% of CNCs.

Figure 35 - Scanning Electron Microscopy of Hydrogels a) without CNC, b) 0.4% CNC and c) 1.0% CNC. Column I shows a magnification of 170 X and column II one of 200 X

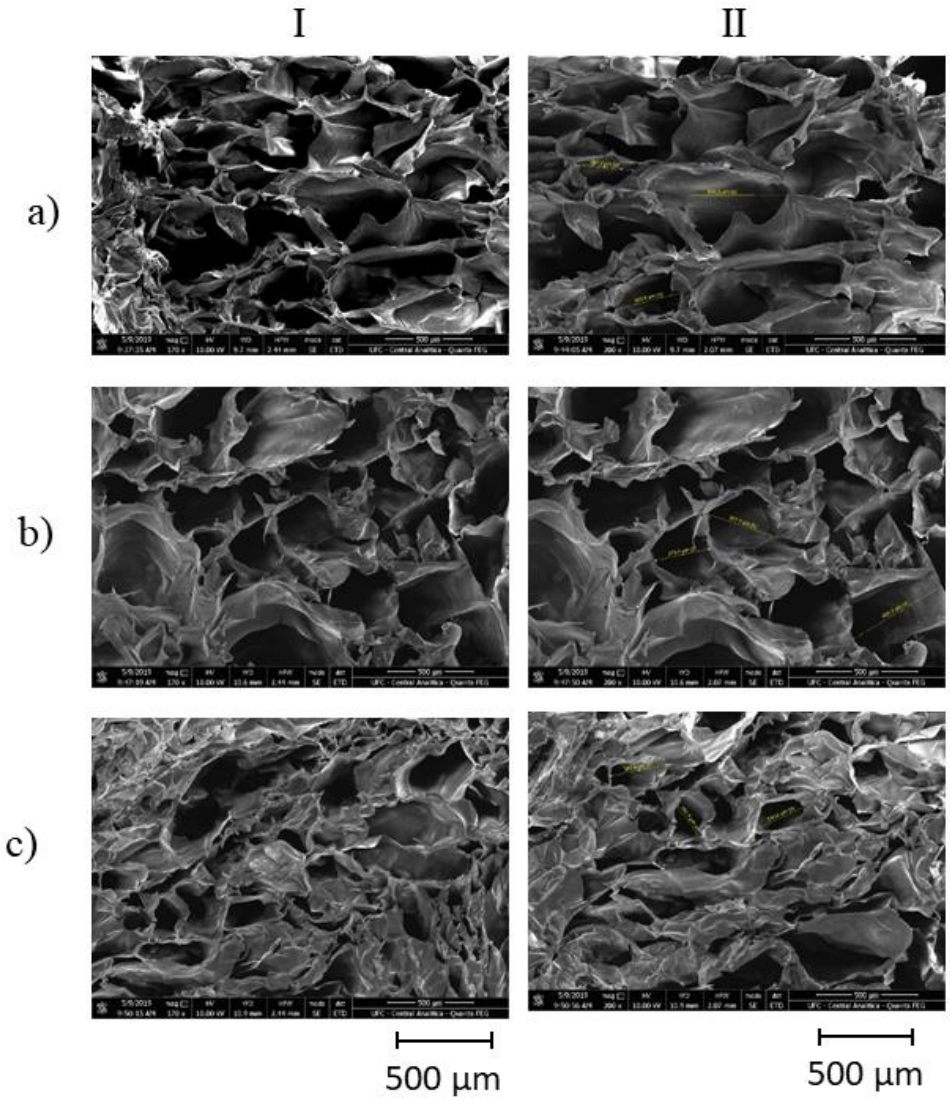

All the hydrogels evaluated had an interconnected pore structure with different diameters and shapes distributed in a heterogeneous form. This type of structural organization is common for hydrogels obtained by lyophilization (LIU et al., 2016; OU et al., 2018; SARKER et al., 2016). It is possible to verify that with the addition of nanocrystals the porous structures became more compact, suggesting that the CNCs contributed to the formation of a denser structure. In fact, the hydrogels with 1.0% of CNC had a mean pore size of 212 µm, with 0.4% of CNC had 377 µm and the hydrogel without CNC had a size of 421 µm. Similar results are reported by DOMINGUES et al., 2015, but they obtained smaller pores and a greater degree

of pore organization, probably because the cellulose nanocrystals used had dual function and acted simultaneously as reinforcing agents of crosslinking agents.

According to BRUŽAUSKAITE et al., 2016, we can classify the hydrogels obtained here as having macroporous structures (100 μm-1 mm). This type of structure is important for distribution, migration and secretion of components of the extracellular matrix, as this rate increases as the pores become larger (ANNABI et al., 2010).

4.4.5 Swelling

The presence of hydrophilic functional groups over the chain of the polymers allows the absorption of polar liquids as water, PBS buffer and biological fluids. One of the characteristics that defines hydrogels as promising biomaterials is their water content, or the degree of swelling. The amount of water or buffer that a hydrogel can absorb/retain in its structure is defined as swelling (CALIARI; BURDICK, 2016). This characteristic can be used to estimate its hydrophilicity as well as the density of crosslinks. These bonds between the adjacent chains of the polymers prevent the dissolution of the hydrogel in the medium even over relatively long periods of time.

Figures 36 and **37** show the swelling of the hydrogels with and without CNC in water and PBS, respectively. PBS was used to mimic physiological conditions. The swelling curves of all hydrogels showed a very similar tendency. The introduction of CNCs led to a small decrease in the degree of swelling, possibly due to the formation of a more cohesive structure. CNCs can interact via hydrogen bonding with the adjacent chains, leading to decrease in the size of the reticule in which water can enter.

For the swelling performed in PBS, it obtained a degree of swelling about 10-12 times lower than in water. Hydrogels with 0.8 and 1.0% CNC had a lower degree of swelling than the non-CNC hydrogel, probably due to the large amount of loading that occupied the pores and prevented the entry of PBS.

Figure 36 - Swelling of the hydrogels with and without CNC in water at room temperature

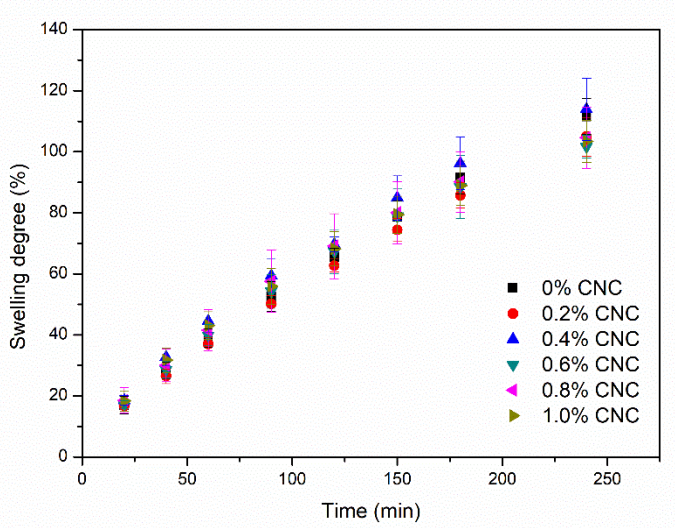

Figure 37 - Swelling of the hydrogels with and without CNC in PBS at room temperature

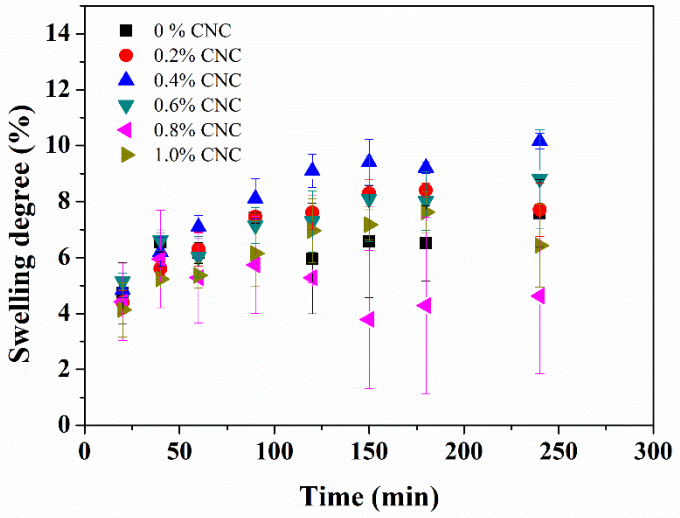

Figure 38 shows a comparison of the macroscopic appearance of the swollen hydrogels in water and in PBS. It is possible to note that the swollen hydrogels in water increase in volume considerably when compared to those swollen in PBS, corroborating the previous swelling curves. It is noteworthy that the swollen hydrogels in PBS cannot alter their volume. This is a noteworthy fact considering that once hydrogels are injected into the site of interest and fills the environment it would not have additional space to occupy.

Another point worth highlighting is that when the hydrogels swelled in PBS, they maintained their physical integrity throughout the study with no visible defects, while the hydrogels that swelled in water are more fragile, eventually collapsing their structure.

Figure 38 - (A) macroscopic appearance of hydrogels after preparation, (B) hydrogels swollen in water by 48 h and (C) size difference of swollen hydrogels reinforced with 1.0% CNC in water and PBS by 48 h

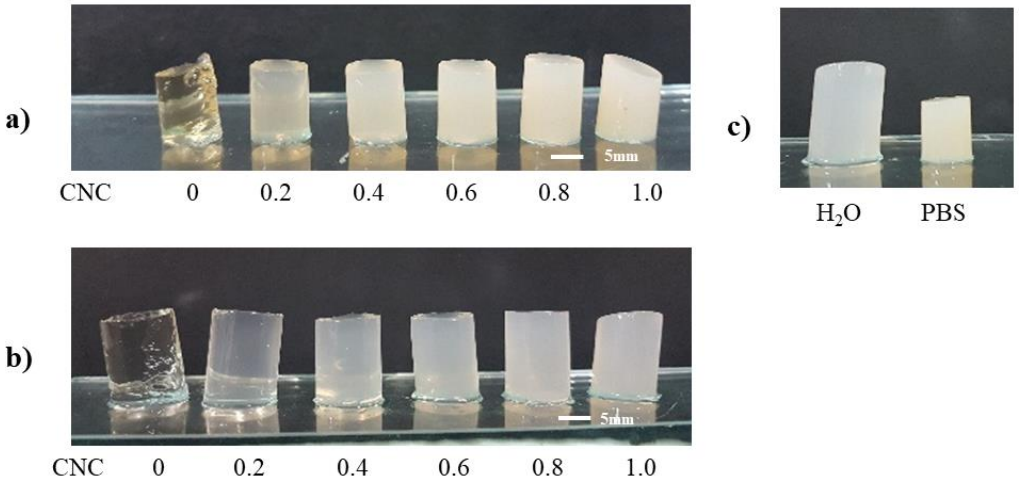

4.4.6 In vitro injectability

One of the advantages associated with the use of injectable hydrogels is their ability to easily encapsulate cells and/or drugs in hydrogel precursor solutions (LI; RODRIGUES; TOMÁS, 2012). This characteristic is associated with the fact that the precursors are in the liquid state and therefore can be administered through a simple injection. The injection procedure depends on the force applied on the plunger, flow uniformity in the bevel and absence of clogging in the cannula (CILURZO et al., 2011) (**Figure 39**). These characteristics define the injectability of a material.

Figure 39 - Parts of the syringe

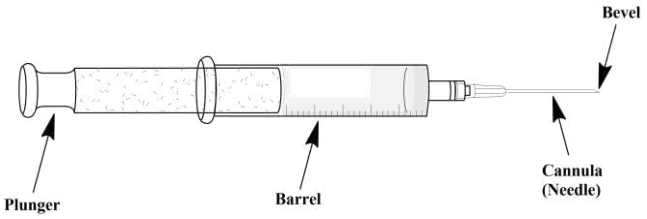

Injectivity of the hydrogels with and without CNCs was evaluated by extruding the components through the cannula of a 1 mL 26G (0.45x13mm) syringe (**Figure 40**). This was only a qualitative experiment to evaluate the extrusability of hydrogels. However, for clinical applications it is necessary to know the amount of force that should be applied to the plunger of the syringe. Although the solutions containing the CNCs clearly showed a higher viscosity as demonstrate previously, the hydrogels prepared from them could easily be injected. The addition of the CNCs did not compromise the injectability. The hydrogel was able to flow without breaking the flow and after injected they maintained their non-flowing form on their own.

In view of the fluid nature of the hydrogels prior to the gelling processor, it can be inferred that they can be administered in irregularly shaped defects and in hard to reach places. It is worth mentioning that for routine clinical applications, small-gauge needles are preferred for reducing site-of-application damage (SAPORITO et al., 2019) and therefore the conditions used in this work (26 G needle) classify the hydrogels obtained as having good injectability for possible clinical applications.

Figure 40 - Injection of the hydrogels from syringes of 1mL 26G (0.45x13mm) to evaluate its injectability

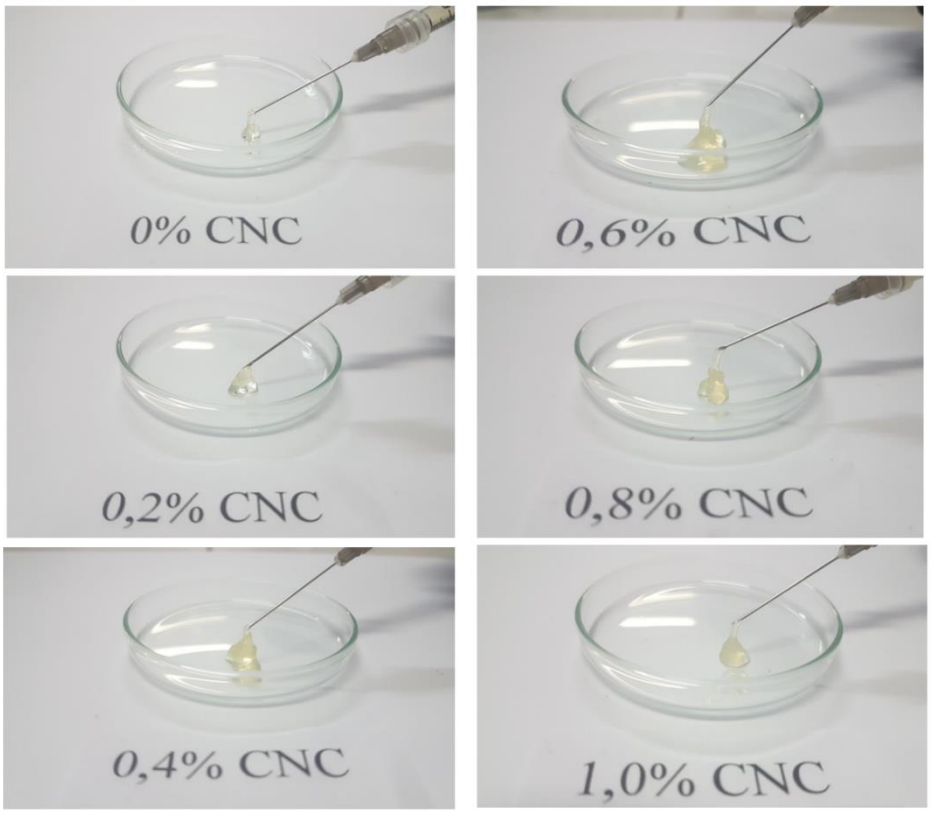

4.4.7 Dynamic Mechanical Analysis

The effect of the CNC addition in the mechanical properties of the hydrogels was evaluated by dynamic mechanical analysis (DMA). The introduction of nanofillers, especially those of natural biocompatible origin, such as nanofibers and nanocrystals, is a way to improve the mechanical properties of hydrogels widely applied nowadays (DOMINGUES; GOMES; REIS, 2014). In addition to changing mechanical properties, these nanoparticles can also modify properties such as swelling, injectability, gelation time and in some cases even biological properties of the hydrogels. According to Hartmann et al., 2019, polymer composites consist of at least two components: the polymer matrix and the (non) polymer reinforcement. This approach has the advantage of being able to combine properties to construct a material with different characteristics of the starting materials (VAGASKÁ et al., 2010).

Figure 41 presents the stress/strain curve for hydrogels with and without CNCs. It is possible to observe that all the hydrogels were within their elastic region, not irreversibly deforming. The deformation of only 5% of the initial length of the samples derives from a technical limitation (displacement of the equipment ~ 3mm). To determine the compression modulus (E) of the gels, a tangent line was drawn in the initial region of the curve and the slope value ($E = \Delta y/\Delta x$) was taken to be equivalent to the compression modulus. The sharper the slope of the tangent line, the greater the compression module of the hydrogel in question.

Figure 41 - Stress/strain curve for the hydrogels showing their elastic region

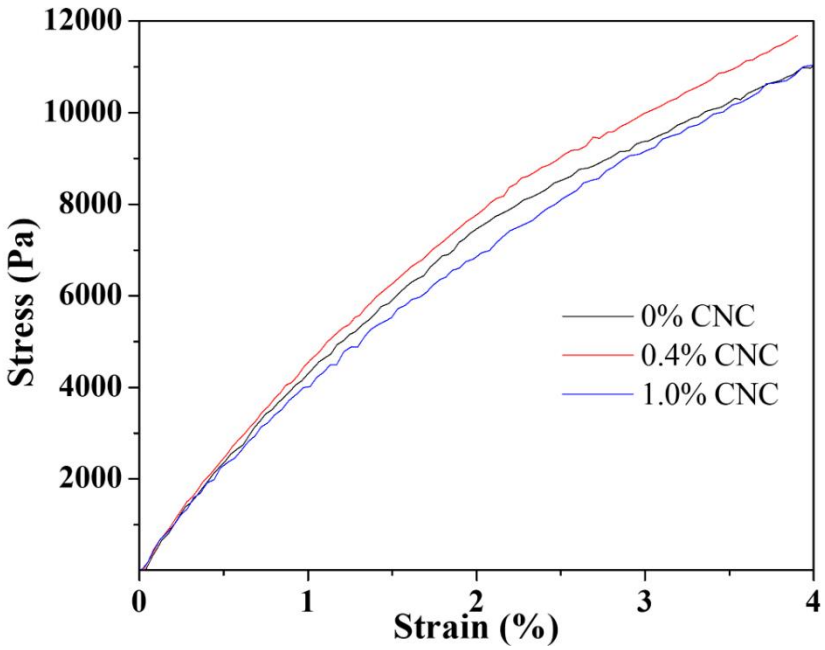

The hypothesis that small amounts of CNCs can reinforce the hydrogel is seen in **Figure 42**. When we compare the hydrogels with 0.2 and 0.4% of CNC it is possible to see an increase of 2.8 and 12.7% in E, indicating that CNCs interact efficiently with the matrix. There was an improvement in the mechanical properties of the hydrogels with CNCs. The possible mechanism that explains the positive effect of the addition of CNCs, under the mechanical properties, relies on the fact that each entrapped CNCs interacts with multiples points of the matrix and multiples points of the matrix interacts with the CNCs, simultaneously (YOUNG, RIAHINEZHAD and AMSDEN, 2019). However, this improvement was not very significant, especially when compared with the works of Yang et al, 2013 and Domingues et al, 2015. The interaction matrix/reinforcing agent in our work is physical, i.e., the reinforcing agent does not chemically bind the matrix. In the case of the works mentioned before, the nanoparticles added to the matrix act simultaneously as reinforcing agents/crosslinking agents and in this way may contribute to a more significant improvement in the mechanical properties.

Figure 42 - Compressive modulus to the hydrogels with different CNC contents

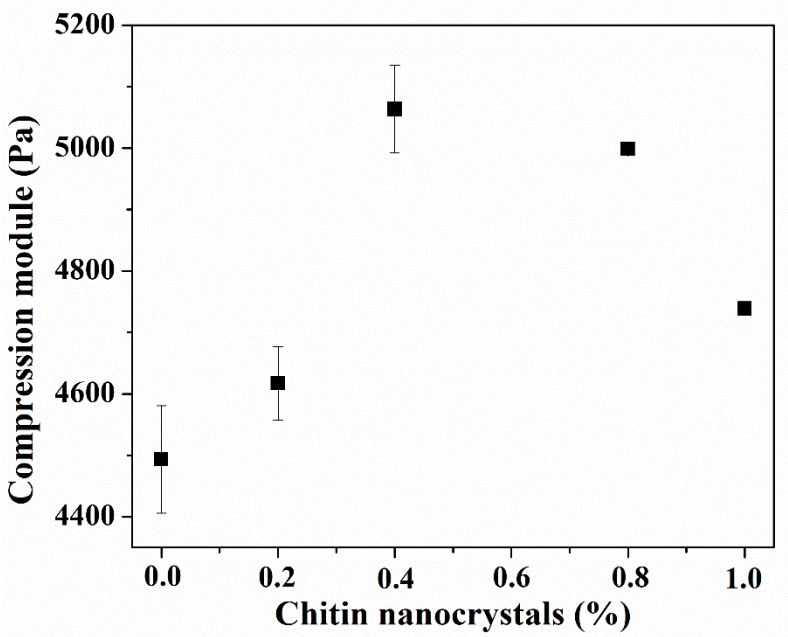

For higher quantities of load (> 0.4%), the CNCs showed an opposite effect with a decrease in E. With this it can be inferred that there is a critical point for load added to the matrix. This general trend has already been reported in other studies that have used nanocrystals as a reinforcing agent. YANG et al., 2013, working with oxidized dextran hydrogels and carboxymethyl cellulose hydrazide functionalized in the formulation of injected hydrogels reinforced with cellulose nanocrystals or oxidized cellulose nanocrystals obtained similar

results for the storage modulus (G'). The introduction of 0.375% (w/v) oxidized cellulose nanocrystals led to the G' of 6700 Pa, a value about 140% higher than for the hydrogel without filler. However, formulations with larger amounts of nanocrystals did not follow the trend of increasing G' and progressively presented smaller values.

DOMINGUES et al., 2015, also obtained similar results. The authors point to the hypothesis that with high amounts of reinforcing agent, there may be a steric blocking of the CNCs. The crosslinking process between the polymers are hindered. Other possibilities would be the self-aggregation of nanocrystals (agglomerate formation) (ZENG et al, 2012) or that of a competitive mechanism, where nanocrystals interact through hydrogen bonding with the hydroxyl groups of adjacent chains locking the structure and decreasing the number of covalent interactions between the chains.

We believe that the greater the amount of CNC, the greater the probability of the existence of aggregation points within the matrix, although it is not possible to verify this hypothesis with the naked eye. Unlike the reinforcement made with nanofibers, in which the load agent is in contact with several points of the matrix simultaneously, the CNCs are smaller in length and aspect ratio. As their quantity increases, we suppose that they tend to interact more with themselves, and with that some micro-points of aggregation emerge that negatively influence the mechanical properties of hydrogels.

4.4.8 Gelation time

The definition of injectable hydrogel considers the in-situ gelation process at the application site; based on this, the sol → gel transition should take place after administration within a time interval ranging from seconds to a few minutes, under physiological conditions (Patenaude, Smeets and Hoare, 2014).

Characterization of injectable hydrogel for its gelation time is critical, once rapid gelling reduces the risk of precursor solutions migrating away from the application site, which would lead to a decrease in the concentration and mechanical properties of the formed hydrogel. However, rapid formation kinetics can also pose challenges associated with the premature formation of the hydrogel before injection (inside the syringe or even inside the needle). On the other hand, we have a slow gelation that can lead to dilution of the precursors by diffusion and

consequently any drug or cell that is using the hydrogel as a vehicle for release (PATENAUDE, SMEETS and HOARE, 2014; LÜ et al., 2015)

The time to hydrogel crosslinking is affected by the kind of method utilized. Generally physical crosslinking took longer periods of time to be complete; even between the chemical crosslinking, there are someone that need hours, like Diels–Alder reactions, to complete (YOUNG, RIAHINEZHAD and AMSDEN, 2019). Other important factor is the initial concentration of the solutions that will be mixed, because it is necessary to have a minimum amount of solid content to promote an appropriate gelation time (YAN et al., 2016)

There are several distinct ways to determine the gelation time. The three most common are: rheologically (crossover between G' and G"), by the tube inversion method (no fluidity is observed visually when the flask is inverted) or by the magnetic bar method (globule formation visible to the naked eye). In view of the application of injectable hydrogels as biomaterials, the above tests are done at 37°C.

In this work the gelation time was determined rheologically by evolution of the elastic or storage modulus (G') and the viscous or loss modulus (G"). In **Figure 43** it is possible to see a comparison between the hydrogel without CNC and the one with 0.4% of CNC. At the beginning, the mixture of both solutions behaved as a viscous fluid (sol), where G" was greater than G'. During the Schiff base formation process, both G' and G" evolved because of the crosslinking process. However, G' increased faster than G" and we can observe a crossover point that is defined as the gel time (SARKER et al., 2014).

We can observe that the addition of the reinforcing agent led to a similar trend to that observed for mechanical analysis, that is, the addition of the CNC had a positive effect for hydrogels with 0.2 and 0.4%, which was reflected by the decrease in gelation time. For the other hydrogels with higher amounts of CNC the effect was contrary (**Figure 44**).

Gelation time for the hydrogel without CNC was 597 s and with the addition of 0.2 and 0.4% CNC, the gelation time decreased to 414 and 377, respectively. Hydrogels with 0.6%, 0.8% and 1.0% had a gelation time of 757, 1157 and 775. From this we can establish that there is no linear relationship between the CNC content and the decrease in the gelling time. There is a limit amount that can be added without compromising the property that is to be improved.

We believe as much as the amount of CNC higher the probability of aggregation points inside the matrix. Another possible explanation would be that with the increase of the

CNC content in the matrix, this would prevent an effective interaction between the hydrogel precursors, which would cause the delay in the formation of bonds that lead to the increase of the storage module in the gelling process. **Figure 45** presents the gelation time curves for all hydrogels prepared in this works**.**

Figure 43 - Gelation time for hydrogel without CNC and with 0.4% of CNC

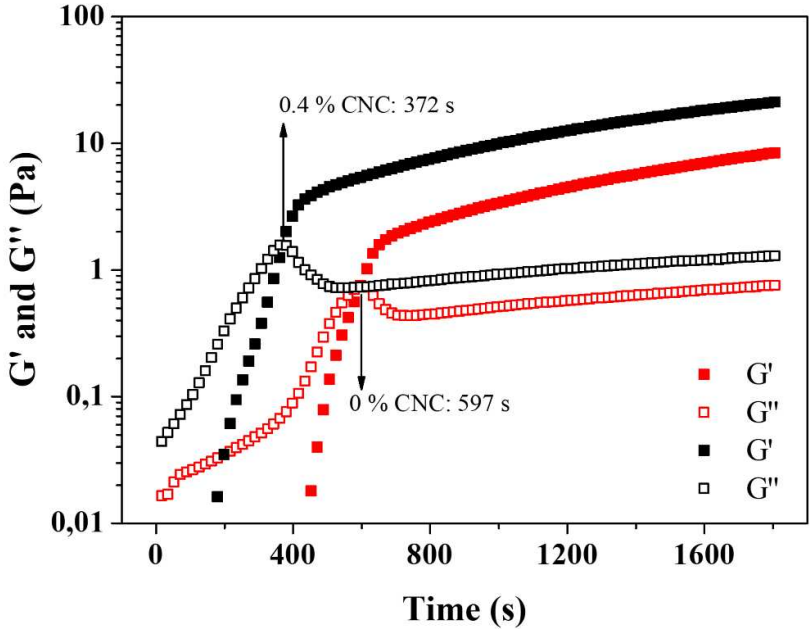

Figure 44 - Gelation time for hydrogels with and without CNC

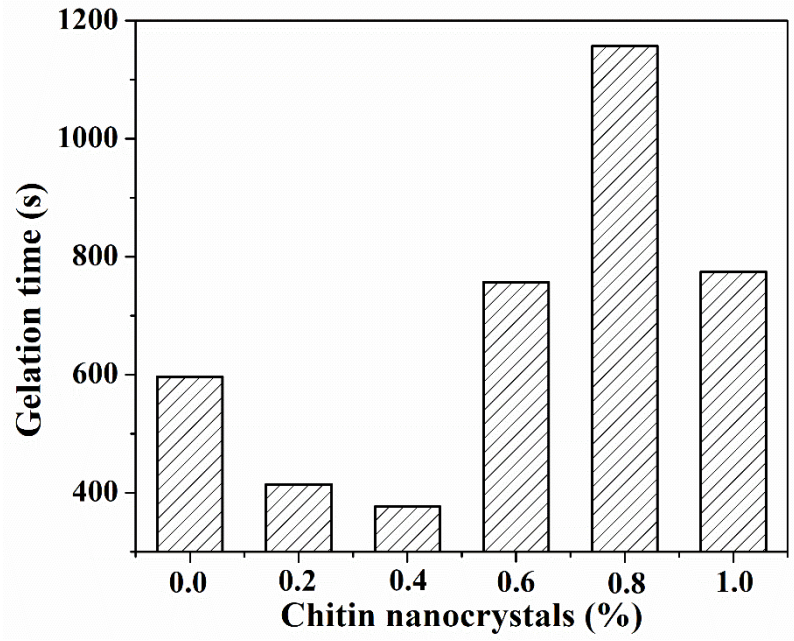

Figure 45 - Gelation time determination for all the conditions studied

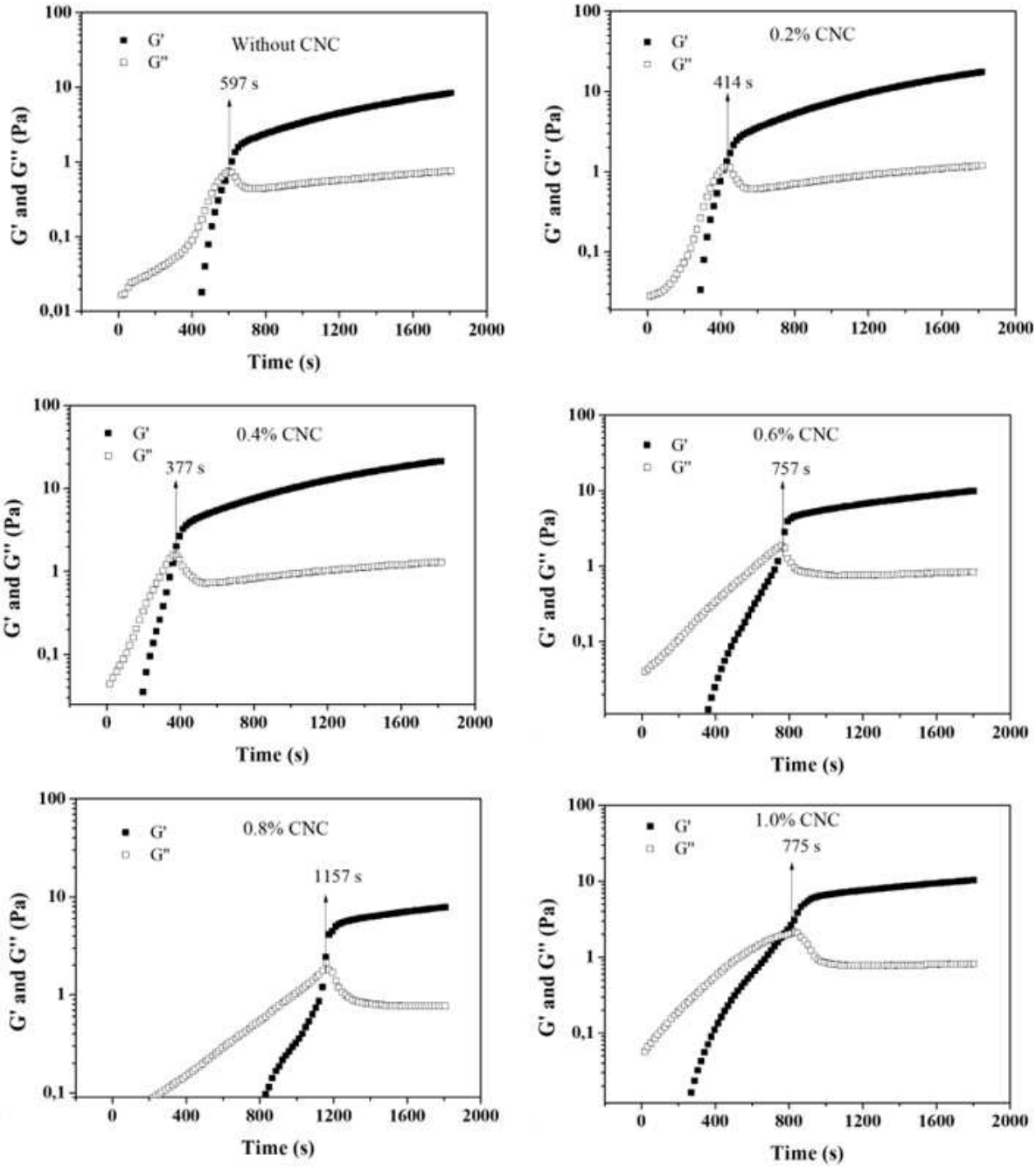

4.4.9 In vitro drug release assay

Figure 46 presents the graph that describes the BSA release profile from the hydrogel matrix. Although the hydrogels containing CNC have a lower percentage of BSA release, they do not seem to show any significant difference between them, that is, the CNC content had no influence on the percentage and speed of BSA release. After 12 h of experiment,

the hydrogel without nanocrystals released 33.4% while the one with 0.4% CNC released 11.6% and the one with 1.0% CNC released 11%, that is, hydrogels with released 3 times less.

From this test it was possible to verify that the hydrogels delay the release of the BSA into the buffer. The addition of the CNCs impacted the release profile, causing a slight decrease in the speed at which the BSA leaves the matrix. This behavior may be related to the existence of a more compact structure that hinders the entry of liquids and, consequently, the release of BSA. This corroborates the previous findings that CNCs have an influence on the final properties of hydrogels.

Figure 46 - BSA release from the hydrogels with and without the nanocrystals

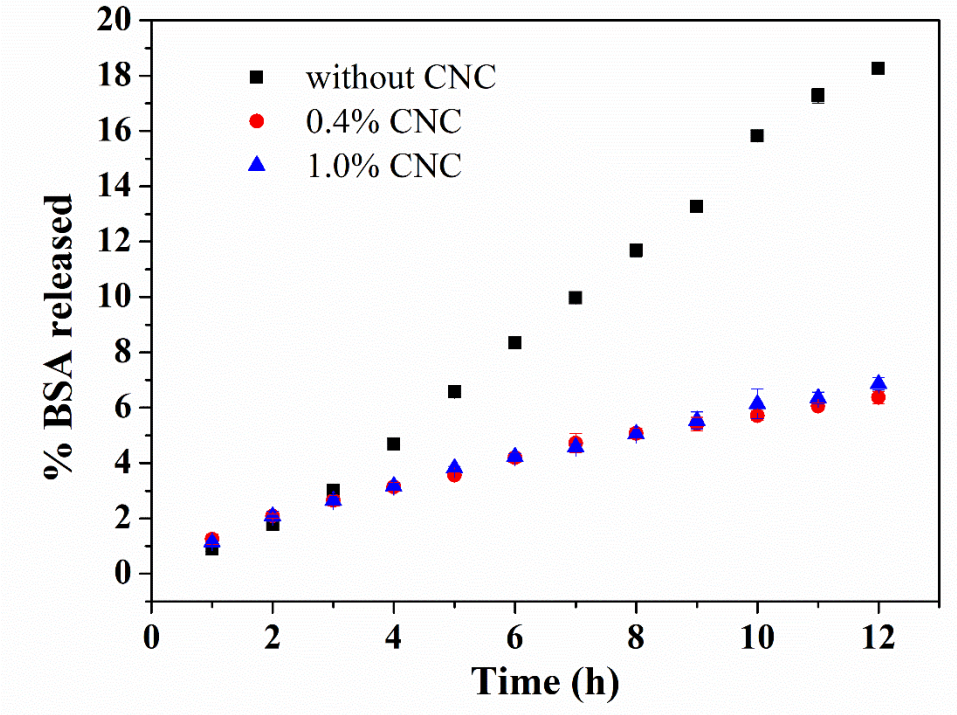

4.4.10 Cell viability

As a possible material that could be applied for a long term and biological finality it's necessary prior to clinical applications to evaluate the cytocompatibility of the hydrogel for some cell line. Another important factor is related to hydrogel promote suitable conditions to cell gas exchange, grow up and eventually differentiation (PIANTANIDA et al., 2019).

A preliminary study of in vitro biocompatibility with L929 fibroblast cell and resazurin was realized using the extracts of the hydrogels according to the procedure described in the ISO 10993-5/2009. Considering that the hydrogel with 0.4% of CNC had the shortest

gelation time and the largest compression modulus, it was selected for the biocompatibility assay. As a comparison, hydrogels without CNC and with 1.0% CNC were also used.

Figure 47 shows the cell viability of the hydrogels analyzed expressly expressed. All hydrogels presented viability greater than 85% when compared to the control sample. The addition of the CNCs seems to have improved the viability. Similar effect was reported by Huang et al, 2015. This result is indicative that the hydrogels with CNC have potential for application as biomaterial.

Figure 47 - Percentage of viable cells after 24 h of experiment

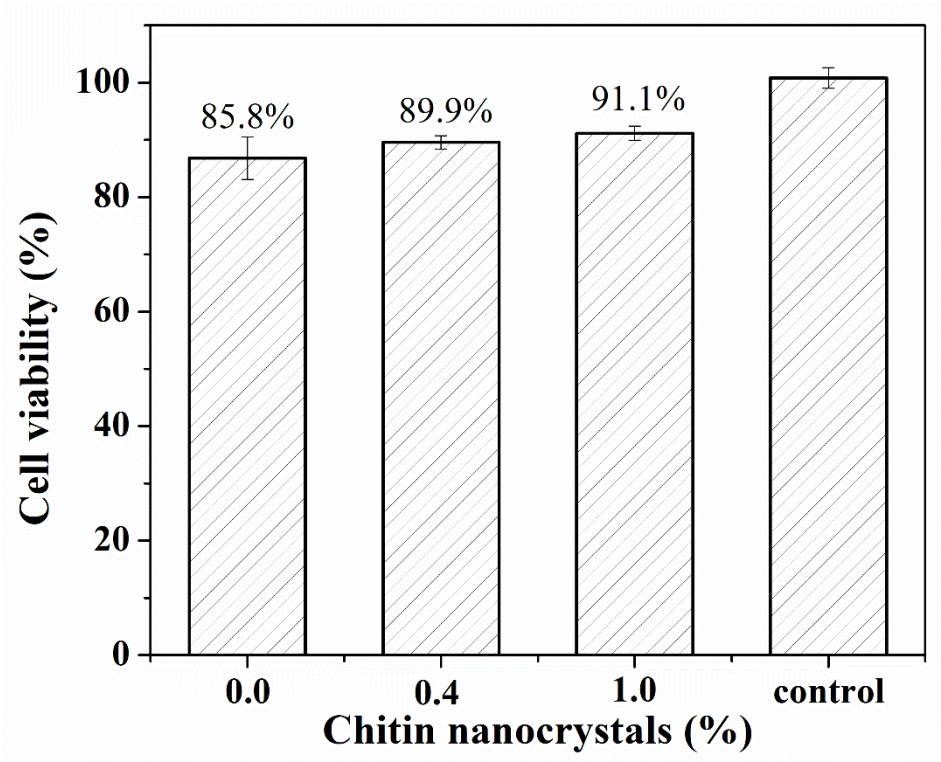

5 CONCLUSIONS

The oxidation process was effective for modifying the structure of galactomannan from *Delonix regia*. The derivative in question showed characteristics for its use as a macrocrosslinker agent for chitosan due to its aldehyde groups. It is assumed that this derivative can also be used with other natural N-nucleophiles such as gelatin, collagen or even synthetic N-nucleophiles as adipic acid dihydrazide.

The derivatization of chitosan proved to be efficient in promoting its solubilization in a wider range of pHs. The presence of the carboxylate groups generated in the reaction, could be readily dissolved guarantee the amphiprotic derivative in water.

The acid extraction process from chitin led to the obtaining of structures (nanocrystals) on the nanometric scale. The nanocrystals showed a predominantly positive surface charge due to the protonation of NH_2 groups that are converted to NH_3^+, during the process of extraction, and thus contribute to the stabilization of the suspension under acid conditions.

The introduction of nanocrystals in the structure of hydrogels led to the obtainment of specimens with an opaque aspect. The higher the content of nanocrystals, the opaquer the hydrogel was. The nanocrystals were dispersed throughout the hydrogel matrix, with no apparent point of agglomeration.

The addition of nanocrystals increased the viscosity of the precursor solution (N-succinyl chitosan) when compared to the chitosan-only solution. However, this increase in viscosity did not significantly compromise the injectability of hydrogels that could be administered using a needle.

The addition of nanocrystals led to a small improvement in the mechanical properties of hydrogels. This can be verified from the obtained compression module values.

The improvement in mechanical properties was only present for hydrogels with 0.2% and 0.4% nanocrystals. Hydrogels loaded with higher amounts of nanocrystals showed the opposite behavior, which can be explained by the possible steric blocking of nanocrystals that competes / prevents the formation of crosslinking points between polymers.

The cytotoxicity assay showed that the hydrogel did not lead to a negative response when in the presence of animal cells.

Based on the set of results obtained, we can infer that with adequate characterization in mechanical and biological terms, the hydrogels of oxidized galactomannan and N-succinyl-chitosan, reinforced by chitin nanocrystals, may have potential as a system for static cell culture or controlled release of drug in a place of interest and it is easy for the procedure to be administered.

REFERENCES

ABREU, C. M. W. S., PAULA, H. C. B., SEABRA, V., FEITOSA, J. P. A., SARMENTO, B., DE PAULA, R.C.M. Synthesis and characterization of non-toxic and thermo-sensitivepoly (N-isopropylacrylamide)-grafted cashew gum nanoparticles as a potential epirubicin delivery matrix. **Carbohydrate Polymers**, *[s.l.]*, v. 154, p. 77-85, 2016.

AHADIAN, S., SADEGHIAN, R. B., SALEHI, S., OSTROVIDOV, S., BAE, H., RAMALINGAM, M., KHADEMHOSSEINI, A. Bioconjugated hydrogels for tissue engineering and regenerative. **Bioconjugate Chemistry**, *[s.l.]*, v. 26, p. 1984−2001, 2015.

AMER, H., NYPELO, T., SULAEVA, I., BACHER, M., HENNIGES, U., POTTHAST, A., ROSENAU, T. Synthesis and Characterization of Periodate-Oxidized Polysaccharides: Dialdehyde Xylan (DAX). **Biomacromolecules**, *[s.l.]*, v. 17, p. 2972-2980, 2016.

ANNABI, N., NICHOL, J. W., ZHONG, X., JI, C., KOSHY, S., KHADEMHOSSEINI, A., DEHGHANI, F. Controlling the Porosity and Microarchitecture of Hydrogels for Tissue Engineering. **TISSUE ENGINEERING: Part B**, *[s.l.]*, v. 16, p.371-383, 2010.

Associação Brasileira de Transplante de Órgãos. Registro Brasileiro de Transplantes. Disponivel em: https://site.abto.org.br/publicacao/xxvii-no-2/. Acesso em: 18 ago. 2021.

BALAKRISHNAN, B., BANERJEE, R. Biopolymer-based hydrogels for cartilage tissue engineering. **Chemical Reviews**, *[s.l.]*, v. 111, p. 4453–4474, 2011.

BAKAIC, E., SMEETS, N. M. B., HOARE, T. Injectable hydrogels based on poly (ethylene glycol) and derivatives as functional biomaterials. **RSC Advances**, *[s.l.]*, v. 5, p. 35469–35486, 2015.

BARAK, S., MUDGIL, D. Locust bean gum: Processing, properties and food applications-A review. **International Journal of Biological Macromolecules**, *[s.l.]*, v. 66 p. 74-80, 2014.

BASHIR, S., TEO, Y. Y., RAMESH, S., RAMESH, K. Physico-chemical characterization of pH-sensitive N-Succinyl chitosan-g-poly (acrylamide-co-acrylic acid) hydrogels and in vitro drug release studies. **Polymer Degradation and Stability**, *[s.l.]*, v. 139, p. 38-54, 2017.

BASHIR, S., TEO, Y.Y., RAMESH, S., RAMESH, K., KHAN, A. A. N-succinyl chitosan preparation, characterization, properties and biomedical applications: a state of the art review. **Reviews in Chemical Engineering**, *[s.l.]*, v. 31, p. 563-597, 2015.

BENAMER, W. Development of Preparative Methods for Chitosan Microparticles. 2012, 172 p.

BELLICH, B., D'AGOSTINO, I., SEMERARO, S., GAMINI, A., CESÀRO, A."The Good, the Bad and the Ugly" of Chitosans. **Marine Drugs**, *[s.l.]*, v. 14, p.1-31, 2016.

BETANCUR-ANCONA, D., PACHECO-AGUIRRE, J., CASTELLANOS-RUELAS, A., CHEL-GUERRERO L. Microencapsulation of papain using carboxymethylated flamboyant

(*Delonix regia*) seed gum. **Innovative Food Science and Emerging Technologies**, *[s.l.]*, v. 12, p. 67–72, 2011.

BROWN, B. N., BADYLAK, S. F. Extracellular matrix as an inductive scaffold for functional tissue reconstruction. **Translational Research**, *[s.l.]*, v. 163, p. 268-285, 2014.

BRUŽAUSKAITE, I., BIRONAITE, D., BAGDONAS, E., BERNOTIENE, E. Scaffolds and cells for tissue regeneration: different scaffold pore sizes-different cell effects. **Cytotechnology**, *[s.l.]*, v.68, p.355–369, 2016.

CALIARI, S. R., BURDICK, J. A. A practical guide to hydrogels for cell culture. **NATURE METHODS**, *[s.l.]*, v. 13, p. 405-414, 2016.

CÁRDENAS, G., CABRERA, G., TABOADA, E., MIRANDA, S. P. Chitin Characterization by SEM, FTIR, XRD, and 13C Cross Polarization/Mass Angle Spinning NMR. **Journal of Applied Polymer Science**, *[s.l.]*, v. 93, p. 1876–1885, 2004.

CAREY, FRANCIS A.; SUNDBERG, RICHARD J. **Advanced Organic Chemistry.** 5th ed. New York: Springer, 2007. 2 v. ISBN 9780387683461.

CHEIRMADURAI, K., THANIKAIVELAN, P., MURALI, R. Highly biocompatible collagen–*Delonix regia* seed polysaccharide hybrid scaffolds for antimicrobial wound dressing. **Carbohydrate Polymers**, *[s.l.]*, v. 137, p. 584–593, 2016.

CHEN, H., XING, X., TAN, H., JIA, Y., ZHOU, T., CHEN, Y., LING, Z., HU, X. Covalently antibacterial alginate-chitosan hydrogel dressing integrated gelatin microspheres containing tetracycline hydrochloride for wound healing. **Materials Science and Engineering C**, *[s.l.]*, v.70, p. 287–295, 2017.

CILURZO, F., SELMIN, F., MINGHETTI, P., ADAMI, M., BERTONI, E., LAURIA, S., MONTANARI, L. Injectability Evaluation: An Open Issue. **AAPS PharmSciTech**, *[s.l.]*, v. 12, p. 604-609, 2011.

DASH, M., CHIELLINI, F., OTTENBRITE, R.M., CHIELLINI, E. Chitosan - A versatile semi-synthetic polymer in biomedical applications. **Progress in Polymer Science**, *[s.l.]*, v. 36, p. 981-1014, 2011.

DE FRANCE, K. J., CHAN, K. J. W., CRANSTON, E. D., HOARE, T. Enhanced mechanical properties in cellulose nanocrystalpoly(oligo ethylene glycol methacrylate) injectable nanocomposite hydrogels through control of physical and chemical cross-linking. **Biomacromolecules**, *[s.l.]*, v. 17, p. 649-660, 2016.

DE FRANCE, K. J., CRANSTON, E. D., HOARE, T. Mechanically Reinforced Injectable Hydrogels. **ACS Applied Polymer Materials**, *[s.l.]*, v. 2, p. 1016–1030, 2020.

DIAS, S. F. L., NOGUEIRA, S. S., DOURADO, F. F., GUIMARÃES, M. A., PITOMBEIRA, N. A. O., GOBBO, G. G., PRIMOD, F. L., DE PAULA, R. C. M., FEITOSA, J. P. A., TEDESCO, A. C., NUNES, L. C. C., LEITE, J. R. S. A., DA SILVA, D. A. Acetylated cashew gum-based nanoparticles for transdermal delivery of diclofenac diethyl amine. **Carbohydrate Polymers**, *[s.l.]*, v. 143, p. 254-261, 2016.

DOMINGUES, R. M. A., GOMES, M. E., REIS, R. L. The Potential of Cellulose Nanocrystals in Tissue Engineering Strategies. **Biomacromolecules**, *[s.l.]*, v. 15, p. 2327-2346, 2014.

DUAN, B., HUANG, Y., LU, A., ZHANG, L. Recent advances in chitin based materials constructed via physical methods. **Progress in Polymer Science**, *[s.l.]*, v. 82, p. 1–33, 2018.

DOMINGUES, R. M., SILVA, M., GERSHOVICH, P., BETTA, S., BABO, P., CARIDADE, S. G., MANO, J. F., MOTTA, A., REIS, R. L., GOMES, M. E. Development of injectable hyaluronic acid/cellulose nanocrystals bionanocomposite hydrogels for tissue engineering applications. **Bioconjugate Chemistry**, *[s.l.]*, v. 26, p. 1571-1581, 2015.

DONG, R., ZHAO, X., GUO, B., MA, P. X. Self-Healing Conductive Injectable Hydrogels with Antibacterial Activity as Cell Delivery Carrier for Cardiac Cell Therapy. **ACS Applied Materials & Interfaces**, *[s.l.]*, v. 8, p. 17138−17150, 2016.

DUFRESNE, A., LIN, N. Characterization of Polysaccharide Nanocrystal-Based Materials in Polysaccharide-Based Nanocrystals: Chemistry and Applications. Edited by Huang, J., Chang, P. R., Lin, N., Dufresne, A. 2014.

Encyclopedia of Nanotechnology. Editors: Professor Bharat Bhushan. ISBN: 978-90-481-9750-7 (Print) 978-90-481-9751-4 (Online), 2012.

El-Sherbiny, I. M., Yacoub, M. H. Hydrogel scaffolds for tissue engineering: Progress and challenges. **Global Cardiology Science and Practice,** *[s.l.]*, v. 38, p. 316-342, 2013.

FITZPATRICK, L. E., MCDEVITT, T. C. Cell-derived matrices for tissue engineering and regenerative medicine applications. **Biomaterials Science**, *[s.l.]*, v. 3, p. 12–24, 2015.

FATHI, A., MITHIEUX, S. M., WEI, H., CHRZANOWSKI, W., VALTCHEV, P., WEISS, A. S., DEHGHANI, F. Elastin based cell-laden injectable hydrogels with tunable gelation, mechanical and biodegradation properties. **Biomaterials**, *[s.l.]*, v. 35, p. 5425-5435, 2014.

GOMEZ, C.G., RINAUDO, M., VILLAR, M.A. Oxidation of sodium alginate and characterization of the oxidized derivatives. **Carbohydrate Polymers**, *[s.l.]*, v. 67, p. 296–304, 2007.

GUAN, X., AVCI-ADALI, M., ALARÇIN, E., CHENG, H., KASHAF, S. S., LI, Y., CHAWLA, A., JANG, H. L., KHADEMHOSSEINI, A. Development of hydrogels for regenerative engineering. **Biotechnology Journal**, *[s.l.]*, v. 12, p. 1-19, 2017.

HAMED, I., ÖZOGUL, F., REGENSTEIN, J. M. Industrial applications of crustacean by-products (chitin, chitosan, and chitooligosaccharides): A review. **Trends in Food Science & Technology**, *[s.l.]*, v. 48, p. 40-50, 2016.

HARTMANN, N. B., HÜFFER, T., THOMPSON, R. C., HASSELLÖV, M., VERSCHOOR, A., DAUGAARD, A. E., RIST, S., KARLSSON, T., BRENNHOLT, N., COLE, M., HERRLING, M. P., HESS, M. C., IVLEVA, N. P., LUSHER, A. L., WAGNER, M. Are We Speaking the Same Language? Recommendations for a Definition and Categorization

Framework for Plastic Debris. **Environmental Science & Technology**, *[s.l.]*, v. 53, p. 1039−1047, 2019.

HEIMBUCK, A. M., PRIDDY-ARRINGTON, T. R., SAWYER, B. J., CALDORERA-MOORE, M. E. Effects of post-processing methods on chitosan-genipin hydrogel properties. **Materials Science & Engineering C**, *[s.l.]*, v. 98, p. 612-618, 2019.

HOSSEINKHANI, H., HONG, P-D., YU. D-S., Self-assembled proteins and peptides for regenerative medicine. **Chemical Reviews**, *[s.l.]*, v. 113, p. 4837-4861, 2013.

HUANG, Q., ZOU, Y., ARNO, M. C., CHEN, S., WANG, T., GAO, J., DOVE, A. P., DU, J. Hydrogel scaffolds for differentiation of adipose derived stem cells. **Chemical Society Reviews**, *[s.l.]*, v. 46, p. 6255—6275, 2017.

HUANG, Y., YAO, M., ZHENG, X., LIANG, X., SU, X., ZHANG, Y., LU, A., ZHANG, L. Effects of chitin whiskers on physical properties and osteoblast culture of alginate based nanocomposite hydrogels. **Biomacromolecules**, *[s.l.]*, v. 16, p. 3499-3507, 2015.

HUANG, W., WANG, Y., CHEN, Y., ZHAO, Y., ZHANG, Q., ZHENG, X., CHEN, L., ZHANG, L. Strong and Rapidly Self-Healing Hydrogels: Potential Hemostatic Materials. **Advanced Healthcare Materials,** *[s.l.]*, v. 5, p. 2813–2822, 2016.

HU, W., WANG, Z., XIAO, Y., ZHANG, S., WANG, J. Advances in crosslinking strategies of biomedical hydrogels. **Biomaterials Science**, *[s.l.]*, v.,7, p. 843-855, 2019.

HUNT, J. A., CHEN, R., VEEN, T. V., BRYAN, N. Hydrogels for tissue engineering and regenerative medicine. **Journal of Materials Chemistry B**, *[s.l.]*, v. 2, p. 5319–5338, 2014.

JAYAKUMAR, R., PRABAHARAN, M., NAIR, S. V., TOKURA, S., TAMURA, H., SELVAMURUGAN, N. Novel carboxymethyl derivatives of chitin and chitosan materials and their biomedical applications. **Progress in Materials Science**, *[s.l.]*, v. 55, p. 675-709, 2010.

JIN, T., LIU, T., LAM, E., MOORES, A. Chitin and chitosan on the nanoscale. **Nanoscale Horizons**, *[s.l.]*, v. 6, p. 505–542, 2021.

KARAGEORGIOU, V., KAPLAN, D. Porosity of 3D biomaterial scaffolds and osteogenesis. **Biomaterials**, *[s.l.]*, v.26 p. 5474–5491, 2005.

KRISTIANSEN, K. A., POTTHAST, A., CHRISTENSEN, B. E. Periodate oxidation of polysaccharides for modification of chemical and physical properties. **Carbohydrate Research**, *[s.l.]*, v. 345, p. 1264-1271, 2010.

KYZAS, G. Z., SIAFAKA, P. I., PAVLIDOU, E. G., CHRISSAFIS, K. J., BIKIARIS, D. N. Synthesis and adsorption application of succinyl-grafted chitosan for the simultaneous removal of zinc and cationic dye from binary hazardous mixtures. **Chemical Engineering Journal**, *[s.l.]*, v. 259, p. 438–448, 2015.

KLEIN, D. Organic Chemistry. Vol. 2, United States of America, 2016.

LANGER, R., VACANTI, J. P. Tissue Engineering. **Science**, *[s.l.]*, v. 260, p. 920–926, 1993.

LANGHANS, S. A. Three-Dimensional in Vitro Cell Culture Models in Drug Discovery and Drug Repositioning. **Frontiers in Pharmacology**, *[s.l.]*, v. 9, p. 1-14, 2018.

LI, Y., RODRIGUES, J., TOMÁS, T. Injectable and biodegradable hydrogels: gelation, biodegradation and biomedical applications. **Chemical Society Reviews**, *[s.l.]*, v. 41, p. 2193-2221, 2012.

LI, M-C., WU, Q., SONG, K., FRENCH, A. D., MEI, C., LEI, T. pH-Responsive Water-Based Drilling Fluids Containing Bentonite and Chitin Nanocrystals. **ACS Sustainable Chem. Eng**, *[s.l.]*, v. 6, p. 3783–3795, 2018.

LARBI, F., GARCÍA, A., DEL VALLE, L. J., HAMOU, A., PUIGGALÍ, J., BELGACEM, N., BRAS, J. Comparison of nanocrystals and nanofibers produced from shrimp shell α-chitin: From energy production to material cytotoxicity and Pickering emulsion properties. **Carbohydrate Polymers**, *[s.l.]*, v. 196, p. 385–397, 2018

LIANG, Y., ZHAO, X., MA, P. X., GUO, B., DU, Y., HAN, X. pH-responsive injectable hydrogels with mucosal adhesiveness based on chitosan-grafted-dihydrocaffeic acid and oxidized pullulan for localized drug delivery. **Journal of Colloid and Interface Science**, *[s.l.]*, v. 536, p. 224–234, 2019.

LIOW, S. S., DOU, Q., KAI, D., KARIM, A. A., ZHANG, K., XU, F., LOH, X. J. Thermogels: In Situ Gelling Biomaterial. **ACS Biomaterials Science & Engineering**, *[s.l.]*, v. 2, p. 295−316, 2016.

LIN, Z-T., SONG, K., BIN, J-P., LIAO, Y-L., JIANG, G-B. Characterization of polymer micelles with hemocompatibility based on N-succinyl-chitosan grafting with long chain hydrophobic groups and loading aspirin. **Journal of Materials Chemistry**, *[s.l.]*, v. 21, p. 19153–19165, 2011.

LIU, H., LI, C., WANG, B., SUI, X., WANG, L., YAN, X., XU, H., ZHANG, L., ZHONG, Y., MAO, Z. Self-healing and injectable polysaccharide hydrogels with tunable mechanical properties. **Cellulose**, *[s.l.]*, v. 25, p. 559-571, 2018a.

LIU, Y., LIU, M., YANG, S., LUO, B., ZHOU, C. Liquid Crystalline Behaviors of Chitin Nanocrystals and Their Reinforcing Effect on Natural Rubber. **ACS Sustainable Chemistry & Engineering**, *[s.l.]*, v. 6, p. 325−336, 2018b.

LIU, M., ZENG, X., MA, C., YI, H., ALI, Z., MOU, X., LI, S., DENG, Y., HE, N. Injectable hydrogels for cartilage and bone tissue engineering. **Bone Research**, *[s.l.]*, v. 5, p. 1-20, 2017.

LIU, M., ZHENG, H., CHEN, J., LI, S., HUANG, J., ZHOU, C. Chitosan-chitin nanocrystal composite scaffolds for tissue engineering. **Carbohydrate Polymers**, *[s.l.]*, v. 152, p. 832–840, 2016.

LOEBEL, C., RODELL, C. B., CHEN, M. H., BURDICK, J. A. Shear-thinning and self-healing hydrogels as injectable therapeutics and for 3D-printing. **Nature Protocols**, *[s.l.]*, v.12, p.1521–1541, 2017.

LÜ, S., GAO, C., XU, X., BAI, X., DUAN, H., GAO, N., FENG, C., XIONG, Y., LIU, M. Injectable and self-healing carbohydrate-based hydrogel for cell encapsulation. **ACS Applied Materials & Interfaces**, *[s.l.]*, v. 7, p. 13029−13037, 2015.

MAIA, J., CARVALHO, R. A., COELHO, J. F. J., SIMÕES, P. N., GIL, M. H. Insight on the periodate oxidation of dextran and its structural vicissitudes. **Polymer**, *[s.l.]*, v. 52, p. 258-265, 2011.

MAIA, J., FERREIRA, L., CARVALHO, R., RAMOS, M. A., GIL, M. H. Synthesis and characterization of new injectable and degradable dextran-based hydrogels. **Polymer**, *[s.l.]*, v. 46, p. 9604–9614, 2005.

MAO, A. S., MOONEY, D. J. Regenerative medicine: Current therapies and future directions. **Proceedings of the National Academy of Sciences**, *[s.l.]*, v. 112, p. 14452–14459, 2015.

MARCHESSAULT, R. H., MOREHEAD, F. F., WALTER, N. M. Liquid crystal systems from fibrillar polysaccharides. **Nature**, *[s.l.]*, v. 184, p. 632 – 633, 1959.

MATHEW, A. P., UTHAMAN, S., CHO, K-H., CHO, C-S., PARK, I-K. Injectable hydrogels for delivering biotherapeutic molecules. **International Journal of Biological Macromolecules**, *[s.l.]*, v. 110, p. 17–29, 2018.

MITSUHASHI, K., QI, P., TAKAHASHI, A., OHTA, S., ITO, T. Prevention of postoperative peritoneal adhesions in rats with sidewall defect-bowel abrasions using metal ion-crosslinked N-succinyl chitosan hydrogels. **Reactive and Functional Polymers**, *[s.l.]*, v. 145, p. 104374, 2019.

MOREIRA, C. D. F., CARVALHO, S. M., MANSUR, H. S., PEREIRA, M. M. Thermogelling chitosan-collagen**-**bioactive glass nanoparticle hybrids as potential injectable systems for tissue engineering. **Materials Science and Engineering C**, *[s.l.]*, v. 58, p. 1207-1216, 2016.

MÜNSTER, L., VÍCHA, J., KLOFÁČ, J., MASAŘ, M., KUCHARCZYK, P., KUŘITKA, I., Stability and aging of solubilized dialdehyde cellulose. **Cellulose**, *[s.l.]*, v. 24, p. 2753–2766, 2017.

NETO, E. M., SOMBRA, V. G., RICHTER, A. R., ABREU, C. M. W. S., MACIEL, J. S., CUNHA, P. L. R., ONO, L., SIERAKOWSKI, M. R., FEITOSA, J. P. A., DE PAULA, R. C. M. Chemically sulfated galactomannan from *Dimorphandra gardneriana* seed: Characterization and toxicity evaluation. **Carbohydrate Polymers,** *[s.l.]*, v. 101, p. 1013-1017, 2014.

OU, X., ZHENG, J., ZHAO, X., LIU, M. Chemically Cross-Linked Chitin Nanocrystal Scaffolds for Drug Delivery. **ACS Applied Nano Materials**, *[s.l.]*, v. 12, p. 6790-6799, 2018.

ORYAN, A., SAHVIEH, S. Effectiveness of chitosan scaffold in skin, bone and cartilage healing. **International Journal of Biological Macromolecules**, *[s.l.]*, v. 104, p.1003–1011, 2017.

PAILLET, M., DUFRESNE, A. Chitin Whisker Reinforced Thermoplastic Nanocomposites. **Macromolecules**, *[s.l.]*, v. 34, p. 6527- 6530, 2001.

PATENAUDE, M., HOARE, T. Injectable, Mixed Natural-Synthetic Polymer Hydrogels with Modular Properties. **Biomacromolecules**, *[s.l.]*, v. 13, p. 369−378, 2012.

PATENAUDE, M., SMEETS, N. M. B., HOARE, T. Designing Injectable, Covalently Cross-Linked Hydrogels for Biomedical Applications. **Macromolecular Rapid Communications**, *[s.l.]*, v. 35, p. 598−617, 2014.

PIANTANIDA, E., ALONCI, G., BERTUCCI, A., DE COLA, L. Design of Nanocomposite Injectable Hydrogels for Minimally Invasive Surgery. **Accounts of Chemical Research**. *[s.l.]*, v. 52, p. 2101−2112, 2019.

PLAPPERT, S. F., QURAISHI, S., PIRCHER, N., MIKKONEN, K. S., VEIGEL, S., KLINGER, K. M., POTTHAST, A., ROSENAU, T., LIEBNER, F. W. Transparent, Flexible, and Strong 2,3-Dialdehyde Cellulose Films with High Oxygen Barrier Properties. **Biomacromolecules**, *[s.l.]*, v.19, p.2969-2978, 2018.

PRAJAPATI, V. D., JANI, G. K., MORADIYA, N. G., RANDERIA, N. P., NAGAR, B. J., NAIKWADI, N. N., VARIYA, B. C. Galactomannan: A versatile biodegradable seed polysaccharide. **International Journal of Biological Macromolecules**, *[s.l.]*, v. 60, p. 83-92, 2013.

QU, J., ZHAO, X., MA, P. X., GUO, B. Injectable antibacterial conductive hydrogels with dual response to an electric field and pH for localized ‘‘smart” drug release. **Acta Biomaterialia**, *[s.l.]*, v. 72,55–69, 2018.

Qu, J., Zhao, X., Liang, Y., Xu, Y., Ma, P. X., Guo, B. Degradable conductive injectable hydrogels as novel antibacterial, antioxidant wound dressings for wound healing. **Chemical Engineering Journal**, *[s.l.]*, v. 362, p. 548–560, 2019.

RANA, D., ZREIQAT, H., BENKIRANE-JESSEL, N., RAMAKRISHNA, S., RAMALINGAM, M. Development of decellularized scaffolds for stem cell-driven tissue engineering. **Journal of Tissue Engineering and Regenerative Medicine**, *[s.l.]*, v. 11, p. 942–965, 2017.

REAKASAME, S., BOCCACCINI, A. R. Oxidized Alginate-Based Hydrogels for Tissue Engineering. **Biomacromolecules**, *[s.l.]*, v. 19, p. 3−21, 2018

REN, Y., ZHAO, X., LIANG, X., MA, P. X., GUO, B. Injectable hydrogel based on quaternized chitosan, gelatin and dopamine as localized drug delivery system to treat Parkinson’s disease. **International Journal of Biological Macromolecules**, *[s.l.]*, v. 105, p. 1079–1087, 2017.

RINAUDO, M. New way to crosslink chitosan in aqueous solution. **European Polymer Journal**, *[s.l.]*, v. 46, p. 1537–1544, 2010.

RINAUDO, M. Chitin and chitosan: Properties and applications. **Progress in Polymer Science**, *[s.l.]*, v. 31, p. 603-632, 2006.

SALDIN, L. T., CRAMER, M. C., VELANKAR, S. S., WHITE, L. J., BADYLAK, S. F. Extracellular matrix hydrogels from decellularized tissues: Structure and function. **Acta Biomaterialia**, *[s.l.]*, v. 49, p. 1–15, 2017.

SAPORITO, F., BAUGH, L. M., ROSSI, S., BONFERONI, M. C., PEROTTI, C., SANDRI, G., BLACK, L., FERRARI, F. In Situ Gelling Scaffolds Loaded with Platelet Growth Factors to Improve Cardiomyocyte Survival after Ischemia. **ACS Biomaterials Science** & **Engineering,** *[s.l.]*, v. 5, p. 329−338, 2019.

SARKER, B., LI, W., ZHENG, K., DETSCH, R., BOCCACCINI, A. R. Designing Porous Bone Tissue Engineering Scaffolds with Enhanced Mechanical Properties from Composite Hydrogels Composed of Modified Alginate, Gelatin, and Bioactive Glass. **ACS Biomaterials Science & Engineering,** *[s.l.]*,v. 2, p. 2240−2254, 2016.

SARKER, B., PAPAGEORGIOU, D. G., SILVA, R., ZEHNDER, T., GUL-E-NOOR, F., BERTMER, M., KASCHTA, J., CHRISSAFIS, K., DETSCHA, R., BOCCACCINI A. R. Fabrication of alginate–gelatin crosslinked hydrogel microcapsules and evaluation of the microstructure and physico-chemical properties. **Journal of Materials Chemistry B**, *[s.l.]*, v. 2, p. 1470–1482, 2014.

SCAFFARO, R., BOTTA, L., LOPRESTI, F., MAIO, A., SUTERA, F. Polysaccharide nanocrystals as fillers for PLA based nanocomposites. **Cellulose**, *[s.l.]*, v. 24, p. 447–478, 2017

SHEN, X., SHAMSHINA J. L., BERTON, P., GURAUC, G., ROGERS, R. D. Hydrogels based on cellulose and chitin: fabrication, properties, and applications. **Green Chemistry**, *[s.l.]*, v. 18, p. 53–75, 2016.

SILVA, C. R., BABO, P. S., GULINO, M., COSTA, L., OLIVEIRA, J. M., SILVA-CORREIA, J., DOMINGUES, R. M. A., REIS, R. L., GOMES, M. E. Injectable and tunable hyaluronic acid hydrogels releasing chemotactic and angiogenic growth factors for endodontic regeneration. **Acta Biomaterialia**, *[s.l.]*, v. 77, p. 155–171, 2018.

SINHA, V.R., KUMRIA, R. Polysaccharides in colon-specific drug delivery. **International Journal of Pharmaceutics**, *[s.l.]*, v. 224, p. 19 –38, 2001.

SINGH, Y. P., MOSES, J. C., BHARDWAJ, N., MANDA, B. B. Injectable hydrogels: a new paradigm for osteochondral tissue engineering. **Journal of Materials Chemistry B**, *[s.l.]*, v.6, p. 5499-5529, 2018.

SIQUEIRA, N. M., PAIVA, B., CAMASSOLA, M., ROSENTHAL-KIM, E. Q., GARCIA, K. C., DOS SANTOS, F. P., SOARES, R. M. D. Gelatin and galactomannan-based scaffolds: Characterization and potential for tissue engineering applications. **Carbohydrate Polymers**, *[s.l.]*, v. 133, p. 8–18, 2015.

SIRVIÖ, J. A., LIIMATAINEN, H., VISANKO, M., NIINIMÄKI, J. Optimization of dicarboxylic acid cellulose synthesis: Reaction stoichiometry and role of hypochlorite scavengers**. Carbohydrate Polymers**, *[s.l.]*, v. 114, p. 73–77, 2014.

TANG, F., LV, L., LU, F., RONG, B., LI, Z., LU, B., YU, K., LIU, J., DAI, F., WU, D., LAN, G. Preparation and characterization of N-chitosan as a wound healing accelerator. **International Journal of Biological Macromolecules,** *[s.l.]*, v. 93, p. 1295–1303, 2016.

THAKUR, A., JAISWAL, M. K., PEAK, C. W., CARROW, J. K., GENTRY, J., DOLATSHAHI-PIROUZ, A., GAHARWAR, A. K. Injectable shear-thinning nanoengineered hydrogels for stem cell delivery. **Nanoscale**, *[s.l.]*, v. 8, p. 12362-12372, 2016.

VAGASKÁ, B., BAČÁKOVÁ, L., FILOVÁ, E., BALÍK, K. Osteogenic Cells on Bio-Inspired Materials for Bone Tissue Engineering. **Physiological Research**, *[s.l.]*, v. 59, p. 309-322, 2010.

WANG, Q., CHEN, S., CHEN, D. Preparation and characterization of chitosan based injectable hydrogels enhanced by chitin nano-whiskers. **Journal of the Mechanical Behavior of Biomedical Materials**, *[s.l.]*, v. 65, p. 466-477, 2017.

WANG, S., OOMMEN, P. O., YAN, H., VARGHESE, P. O. Mild and efficient strategy for site-selective aldehyde modification of glycosaminoglycans: tailoring hydrogels with tunable release of growth factor. **Biomacromolecules**, *[s.l.]*, v. 14, p. 2427−2432, 2013.

WANG, X., GU, Z., QIN, H., LI, L., YANG, X., YU, X. Crosslinking effect of dialdehyde starch (DAS) on decellularized porcine aortas for tissue engineering. **International Journal of Biological Macromolecules**, *[s.l.]*, v. 79, p. 813–821, 2015.

WEI, Z., YANG, J. H., LIU, Z. Q., XU, F., ZHOU, J. X., ZRÍNYI, M., OSADA, Y., CHEN, Y. M. Novel Biocompatible Polysaccharide-Based Self-Healing Hydrogel. **Advanced Functional Materials***, [s.l.]*, v. 25, p. 1352–1359, 2015.

XING, L., SUN, J., TAN, H., YUAN, G., LI, J., JIA, Y., XIONG, D., CHEN, G., LAI, J., LING, Z., CHEN, Y., NIU, X. Covalently polysaccharide-based alginate/chitosan hydrogel embedded alginate microspheres for BSA encapsulation and soft tissue engineering. **International Journal of Biological Macromolecules**, *[s.l.]*, v. 127, p. 340–348, 2019.

XU, Y., LI, L., WANG, H., YU, X., GU, Z., HUANG, C., PENG, H. In vitro cytocompatibility evaluation of alginate dialdehyde for biological tissue fixation. **Carbohydrate Polymers**, *[s.l.]*, v. 92, p. 448–454, 2013.

XU, Z., BRATLIE, K. M. Click Chemistry and Material Selection for in Situ Fabrication of Hydrogels in Tissue Engineering Applications. **ACS Biomaterials Science** & **Engineering**, *[s.l.]*, v. 4, p. 2276-2291, 2018.

YAN, S., ZHANG, X., ZHANG, K., DI, H., FENG, L., LI, G., FANG, J., CUI, L., CHEN, X., YIN, J. Injectable *in situ* forming poly(L-glutamic acid) hydrogels for cartilage tissue engineering. **Journal of Materials Chemistry B**, *[s.l.]*, v. 4, p. 947-961, 2016.

YAN, N., CHEN, X. Sustainability: Don't waste seafood waste. **Nature**, *[s.l.]*, v. 524, p. 155−157, 2015.

YAN, S., WANG, T., FENG, L., ZHU, J., ZHANG, K., CHEN, X., CUI, L., YIN, J. Injectable *in Situ* self-cross-linking hydrogels based on poly (L-glutamic acid) and alginate for cartilage tissue engineering. **Biomacromolecules**, *[s.l.]*, v. 15, p. 4495-4508, 2014.

YANG, J-A., YEOM, J., HWANG, B. W., HOFFMAN, A. S., HAHN, S. K. *In situ*-forming injectable hydrogels for regenerative medicine. **Progress in Polymer Science**, *[s.l.]*, v. 39, p. 1973–1986, 2014.

YANG, X., BAKAIC, E., HOARE, T., CRANSTON, D. E. Injectable polysaccharide hydrogels reinforced with cellulose nanocrystals: morphology, rheology, degradation, and cytotoxicity. **Biomacromolecules**, *[s.l.]*, v. 14, p. 4447−4455, 2013.

YANG, X-Y., CHEN, L-H., LI, Y., ROOKE, J. C., SANCHEZ, C., SU, B-L. Hierarchically porous materials: synthesis strategies and structure design. **Chemical Society Reviews***, [s.l.]*, v. 46, p. 481-558, 2017.

YANG, T., QI, H., LIU, P., ZHANG, K. Selective Isolation Methods for Cellulose and Chitin Nanocrystals. **ChemPlusChem**, *[s.l.]*, v. 85, p. 1081–1088, 2020

YADAV, H., MAITI, S. Research progress in galactomannan-based nanomaterials: Synthesis and application. **International Journal of Biological Macromolecules**, *[s.l.]*, v. 163, p. 2113–2126, 2020.

YOUNGSTROM, D. W., BARRETT, J. G., JOSE, R. R., KAPLAN, D. L. Functional characterization of detergent-decellularized equine tendon extracellular matrix for tissue engineering applications, **PLoS ONE**, *[s.l.]*, v. 8, 2013.

YUAN, L., LI, X., GE, L., JIA, X., LEI, J., MU, C., LI, D. Emulsion Template Method for the Fabrication of Gelatin-Based Scaffold with Controllable Pore Structure. **ACS Applied Materials & Interfaces**, *[s.l.]*, v.11, p. 269-277, 2019

YUE, K., DE SANTIAGO, G. T., ALVAREZ, M. M., TAMAYOL, A., ANNABI, N., KHADEMHOSSEINI, A. Synthesis, properties, and biomedical applications of gelatin methacryloyl (GelMA) hydrogels. **Biomaterials**, *[s.l.]*, v. 73, p. 254-271, 2015

YOUNG, S. A., RIAHINEZHAD, H., AMSDEN, B. G. In situ-forming, mechanically resilient hydrogels for cell delivery. **Journal of Materials Chemistry B**, *[s.l.]*, v. 7, p. 5742-5761, 2019.

ZHANG, C., PING, Q., ZHANG, H., SHEN, J. Synthesis and characterization of water-soluble O-succinyl-chitosan. **European Polymer Journal**, *[s.l.]*, v. 39 p. 1629-1634, 2003.

ZHANG, H., COOPER, A. I. Aligned Porous Structures by Directional Freezing. **Advanced Materials**, *[s.l.]*, v. 19, p. 1529–1533, 2007.

ZHAO, H., HEINDEL, N. D. Determination of degree of substitution of formul groups in polyaldehyde dextran by the hydroxylamine hydrochloride method. **Pharmaceutical Research**, *[s.l.]*, v. 8, p. 400-402, 1991.

ZHANG, L., GE, H., XU, M., CAO, J., DAI, Y. Physicochemical properties, antioxidant and antibacterial activities of dialdehyde microcrystalline cellulose. **Cellulose**, *[s.l.]*, v. 24, p. 2287–2298, 2017.

ZHANG, Y. S., KHADEMHOSSEIN, A. Advances in engineering hydrogels. **Science**, *[s.l.]*, v. 356, p. 1-10, 2017.

ZHANG, X., ROLANDI, M. Engineering strategies for chitin nanofibers. **Journal of Materials Chemistry B***, [s.l.]*, v. 5, p. 2547-2559, 2017.

ZHENG, C-X., SUI, B-D., HU, C-H., QIU, X-Y., ZHAO, P., JIN, Y. Reconstruction of structure and function in tissue engineering of solid organs: Toward simulation of natural development based on decellularization. **Journal of Tissue Engineering and Regenerative Medicine,** *[s.l.]*, v. 12, p.1432–1447, 2018.

ZENG, J-B., HE, Y-S., LI, S-L., WANG, Y-Z. Chitin whiskers: an overview. **Biomacromolecules**, *[s.l.]*, v. 13, p. 1-11, 2012.